J. Fluid Mech. (1993), *vol.* 257, *pp.* 229–264

Dynamics of a conducting drop in a time-periodic electric field

By I. S. KANG

Department of Chemical Engineering and Advanced Fluids Engineering Research Center, Pohang Institute of Science and Technology, PO Box 125, Pohang, 790-600 Korea

(Received 11 August 1992 and in revised form 7 June 1993)

The nonlinear dynamical behaviour of a conducting drop in a time-periodic electric field is studied. Taylor's (1964) theory on the equilibrium shape is extended to derive a dynamical equation in the form of an ordinary differential equation for a conducting drop in an arbitrary time-dependent, uniform electric field based on a spheroidal approximation for the drop shape and the weak viscosity effect. The dynamics is then investigated via the classical two-timing analysis and the Poincaré map analysis of the resulting dynamical equation. The analysis reveals that in the neighbourhood of a stable steady solution, an $O(\epsilon^{\frac{1}{3}})$ time-dependent change of drop shape can be obtained from an $O(\epsilon)$ resonant forcing. It is also shown that the probability of drop breakup via chaotic oscillation can be maximized by choosing an optimal frequency for a fixed forcing amplitude. As a preliminary analysis, the effect of weak viscosity on the oscillation frequency modification in a steady electric field is also studied by using the domain perturbation technique. Differently from other methods based on the theory of viscous dissipation, the viscous pressure correction is directly obtained from a consideration of the perturbed velocity field due to weak viscosity.

1. Introduction

One of the interesting free boundary problems is the deformation of fluid interfaces under an applied electric or magnetic field. This problem lies at the core of various applications and has been studied by many investigators. In the present paper, we are concerned with the dynamics of a conducting drop in an electric field. Specifically, we investigate the deformation and breakup of a conducting drop by considering the dynamic response of the drop shape to time-periodic perturbations of an electric field.

The equilibrium shape for a drop in a steady electric field was first obtained by Taylor (1964). He approximated the equilibrium shapes of a conducting drop as spheroids, and applied the normal stress condition at the poles and the equator to determine the shape. By means of two-point approximation, Taylor showed that there exists a limit point (the so-called Taylor limit) in dimensionless electric field strength beyond which no steady-state solution can be obtained. The existence of the limit point has been verified by the numerical solutions of various investigators (Miksis 1981; Basaran & Scriven 1989). Since the work of Taylor, it has been found that there are two branches of stable and unstable solutions when the dimensionless electric field strength is below the Taylor limit.

Another problem of fundamental importance in drop dynamics is the oscillation frequency of a small-amplitude perturbation about the stable steady-state shape in a steady electric field. Motivated by a meteorological interest, Brazier-Smith *et al.* (1971) extended Taylor's spheroidal approximation method to calculate the oscillation

frequency of a conducting drop in an electric field. They showed that the oscillation frequency decreases as the electric field strength increases and becomes zero at the Taylor limit. Although the result of Brazier-Smith *et al.* predicts the frequency modification quite accurately for a wide range of dimensionless elecric field strength, the spheroidal approximation restricts the study to a special form of oscillation mode. On the other hand, there have been several investigations on the frequency modification for the more general form of axisymmetric oscillations in the limit of small electrical field strength. Among them, two works by Sample, Raghupathy & Hendricks (1970) and Morrison, Leavitt & Wortman (1981) are worthy of note. In both analyses, the drop shape was expressed in terms of the Legendre polynomials and the Lagrange equation was solved using approximate expressions for the kinetic and potential energies. Unfortunately, the scaling of small parameters was not clearly identified and the terms of the same order were not systematically retained. As a consequence, their results for the $n = 2$ mode show a discrepancy with the result of Brazier-Smith *et al.* even when the electric field strength is small. Recently, Feng (1990) analysed the same problem by the domain perturbation method with multiple parameters to derive the oscillation frequency of an inviscid drop as a function of electric field strength for the asymptotic case of small strength, and obtained a result that is in good agreement with the simplified models based on the assumption of spheroidal deformations. Feng's result has further been extended to include net charge effects (Feng & Beard 1990) and three-dimensional effects (Feng & Beard 1991*b*).

The dynamics of a drop in a time-dependent electric field has been investigated by very few researchers. Sozou (1972) extended Taylor's (1966) work on the flow field induced by an electric field in and about a liquid drop in an incompressible conducting fluid. He included time-dependent electric fields and gave a number of results in the form of equations with a few cases of numerical results. Later, Morrison *et al.* (1981) calculated the Lagrangian to derive a linearized equation of motion. They considered three types of fields: a static electric field, an alternating electric field, an an amplitude-modulated high-frequency field. Recently, Feng & Beard (1991*a*) studied the oscillation of a conducting drop in an alternating electric field by using the domain perturbation method. In their analysis, a primary resonance occurs in the first-order forced oscillation problem. Under strong excitation, superharmonic, subharmonic, and coupled resonances are revealed in their second-order solution. Although rigorous, their analysis is limited to the near-sphere oscillation, i.e. the base equilibrium state for their analysis is a spherical drop in the absence of an electric field. Consequently, their analysis could not reveal more interesting nonlinear dynamical behaviour such as two-timing oscillatory solutions or indefinite stretching due to the primary resonances.

In this paper, we therefore perform a global analysis of the nonlinear dynamical behaviour of a conducting drop in a time-periodic electric field, the time-averaged electric field strength of which is lower than the Taylor limit. To achieve the goal of the present work, Taylor's (1964) theory on the equilibrium shape is extended to derive a dynamical equation for a conducting drop in an arbitrary time-dependent, uniform electric field based on the spheroidal approximation. Then the dynamics of a conducting drop are investigated via the classical two-timing analysis and the Poincaré map analysis of the resulting dynamical equation.

As we shall see later, one of the most important pieces of information for the study of drop dynamics in a time-periodic field is the intrinsic frequency of oscillation in a steady field. Thus, before going on to the main part of the present work we revisit briefly the problem of oscillation frequency change in a steady electric field in order to extend Feng's (1990) asymptotic formula by including the weak viscous effect.

Differently from other methods based on the theory of viscous dissipation, the viscous pressure correction and the viscous normal stress are obtained directly from consideration of the perturbed velocity field due to weak viscosity. Some results in this preliminary section will be used in a derivation of the dynamical equation as well as in a comparison of results for the effect of weak viscosity on the frequency change derived by two different approximations.

Of particular relevance to the present study is the phase-plane portrait of changes of drop shape in a steady electric field. As we shall see later, Taylor's (1964) result indicates that there exists a homoclinic orbit (or separatrix) in a phase-plane portrait when the viscosity effect is neglected. The homoclinic orbit separates stable oscillatory solutions from unstable solutions that correspond to exponential stretching in the electric field direction. This suggests that the drop shape will be susceptible to a transition from regular to chaotic behaviour upon introduction of a time-periodic modulation of the electric field strength. In fact, the present problem is quite similar to the problem of bubble dynamics in time-periodic straining flows, which was analysed by Kang & Leal (1990). Kang & Leal showed that a bubble in a time-periodic straining flow may exhibit regular or chaotic behaviour depending on the initial conditions and parameters. Thus, in spirit, the work reported here is closely related to the analysis of Kang & Leal (1990).

2. Problem formulation

We consider an incompressible conducting drop of volume $\frac{4}{3}\pi a_0^3$ in vacuum, which is undergoing deformations of shape in the presence of a time-periodic, electric field as shown in figure 1. The electric field away from the drop is uniform and of strength $E_\infty(t)$. The density and viscosity of the fluid are ρ and μ, and the surface of the drop is assumed to be characterized completely by a uniform surface tension γ. Furthermore, we neglect all effects of gravity including the hydrostatic pressure variation in the fluid.

In our analysis, we consider the axisymmetric dynamics of a weakly viscous drop. The dynamics of a weakly viscous drop has usually been studied via the theory of viscous dissipation (e.g. Lamb 1932). However, as shown in previous works (Prosperetti 1977; Kang & Leal 1988; Feng & Beard 1991*a*), the weak viscous effects can also be studied by using the equation of inviscid motion if the viscous pressure correction and the viscous normal stress are included in the boundary condition for the normal stress balance. Thus, we adopt the latter approach and use the electric field and velocity potentials ($\boldsymbol{E} = \nabla\psi$ and $\boldsymbol{u} = \nabla\phi$) in the formulation. We then non-dimensionalize all governing equations and boundary conditions with the following characteristic scales:

$$l_c = a_0, \quad t_c = \left(\frac{\rho a_0^3}{\gamma}\right)^{\frac{1}{2}}, \quad \psi_c = E_\infty(t)\, a_0, \quad \phi_c = \left(\frac{\gamma a_0}{\rho}\right)^{\frac{1}{2}}.$$

The dimensionless governing equations are for the electric field outside the drop

$$\nabla^2\psi = 0, \tag{1}$$

and for the fluid motion inside the drop

$$\nabla^2\phi = 0. \tag{2}$$

For the boundary conditions, in addition to the far-field condition

$$\nabla\psi \to \boldsymbol{e}_x \quad \text{as} \quad r \to \infty, \tag{3}$$

we have at the drop surface,

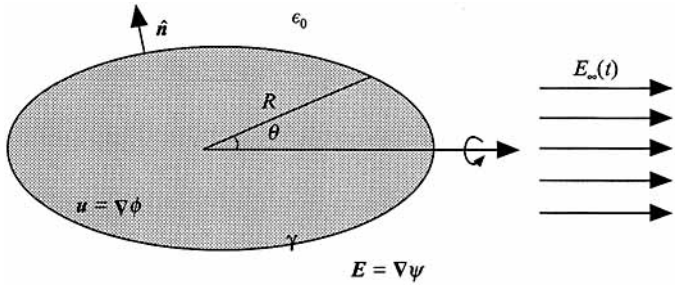

FIGURE 1. A conducting drop in a time-dependent electric field.

(i) kinematic condition:

$$-\frac{1}{|\nabla F|}\frac{\partial F}{\partial t} = \nabla\phi\cdot\hat{\boldsymbol{n}}, \tag{4}$$

(ii) normal stress condition:

$$\tfrac{1}{2}W(t)\,E_n^2 - \frac{\partial\phi}{\partial t} - \tfrac{1}{2}\nabla\phi\cdot\nabla\phi - 2S\frac{\partial^2\phi}{\partial\hat{n}^2} + p_v + G(t) = \nabla\cdot\hat{\boldsymbol{n}}, \tag{5}$$

(iii) infinite-permittivity condition:

$$\psi = \text{constant along the surface}, \tag{6}$$

where $F = r - R(\theta, t)$ is the shape function for the drop surface and $\hat{\boldsymbol{n}}$ is the outward unit normal at the drop surface. In the normal stress condition, E_n denotes the normal component of the electric field, i.e. $E_n = \boldsymbol{n}\cdot\boldsymbol{E} = \partial\psi/\partial\hat{\boldsymbol{n}}$, and $W(t)$ is the time-dependent electrical Weber number defined as

$$W(t) = \frac{\epsilon_0 E_\infty(t)^2 a_0}{\gamma},$$

where ϵ_0 is the electric permittivity in vacuum. The term $-2S(\partial^2\phi/\partial\hat{n}^2)$ represents the viscous normal stress and p_v is the pressure correction due to the weak viscous effect. The dimensionless number S is defined as

$$S = \frac{\mu}{(\rho a_0\gamma)^{\frac{1}{2}}} = \frac{t_c}{a_0^2/(\mu/\rho)} = \frac{t_{c,sur}}{t_{c,vis}}$$

and its physical meaning is the ratio of a surface-tension-based timescale and a timescale for viscous diffusion. For a perfectly conducting drop, the shear stress due to fluid motion at the drop surface should vanish because both the total shear stress and the tangential electric stress are zero at the drop surface (Melcher & Taylor 1969). This vanishing shear stress condition is used to evaluate the viscous correction p_v in (5). In addition to the differential equations and boundary conditions (1)–(6), the solution for the drop shape must satisfy two overall constraints of volume conservation and centre condition. In fact, the time-dependent constant $G(t)$ in (5) is determined by the constraint of volume conservation.

In our formulation, we assumed electrostatic equilibrium at each time. In order for this assumption to be valid, the charge relaxation time τ_r, defined as $\tau_r = \epsilon_0/\sigma_c$ where σ_c is the conductivity of fluid, should be much smaller than the characteristic time for fluid motion t_c, i.e.

$$\left(\frac{\rho a_0^3}{\gamma}\right)^{\frac{1}{2}} \gg \frac{\epsilon_0}{\sigma_c}.$$

As an example, for water at room temperature, $\tau_r \approx 10^{-8}$ s and $t_c \approx 1.2 \times 10^{-7}$ s if $a_0 = 1$ μm (see Nafeh & Brussel 1985). Thus, an electrostatic equilibrium may be safely assumed unless the drop size is extremely small.

3. Results from perturbation analysis for a drop in a steady electric field

Before going on to the main part of the present paper, we touch briefly on the results from the perturbation analysis on the oscillation about the steady shape in a steady electric field (i.e. $W(t) = W = \text{constant}$) in the limit $0 \leqslant W \ll 1$ and $0 \leqslant S \ll 1$. In later sections, the nonlinear dynamical behaviour of a drop in a time-periodic electric field will be studied based on the spheroidal approximation rather than the domain perturbation analysis. However, as we shall see later, one of the most important pieces of information for the study of drop dynamics in a time-periodic field is the intrinsic frequency of oscillation in a steady field. Thus, it would be better if we have the results for the frequency modification obtained by two different approximations. In fact, some results in this section will be frequently referred to for various purposes such as derivation of the dynamical equation and comparison of the results from two different approximations. Thus, we want to discuss several results from the perturbation analysis to render this work more self-contained.

3.1. *Oscillation of a weakly viscous drop*

For axisymmetric oscillations of an inviscid drop, a rigorous asymptotic formula for the frequency modification due to an electric field was first obtained by Feng (1990). He used the domain perturbation method with multiple timescales to obtain the result (equation (4.28) in Feng 1990), which can be expressed compactly after some algebra as

$$\frac{\omega_n}{\omega_{n0}} = 1 - \frac{9(2n^5+23n^4+21n^3-17n^2-7n-2)}{8(2n-1)(2n+1)(2n+3)(n-1)(n+2)} W + O(W^2), \tag{7}$$

where ω_{n0} is the frequency of the nth mode for the case of no electric field and it is

$$\omega_{n0} = ((n-1)n(n+2))^{\frac{1}{2}}.$$

In the present section, the weak viscosity effect is considered to extend Feng's result. Morrison *et al.* (1981) considered the same problem to extend the Rayleigh theory of oscillation of liquid drops. They used Rayleigh's dissipation function to derive the effect of viscosity. However, unfortunately their asymptotic formula for the frequency modification due to the electric field is not correct because of the reason mentioned in the introduction. Differently from the previous works based on the dissipation theory, in the present work the viscosity effect is considered via the viscous pressure correction and the viscous normal stress in the normal stress condition. Particular emphasis will be given to how the vorticity is generated at the curved drop surface due to the vanishing shear stress condition and how the pressure is affected by the generated vorticity. Furthermore, the physics underlying the damping effect by the viscous pressure correction and the viscous normal stress will be clearly explained.

In the derivation of the effect of viscosity, we adopt the standard domain perturbation method, which is slightly different from but equivalent to the method that was used by Feng. Instead of adopting multiple timescales, just a single timescale is used in this work. In our method, the solution is expanded as

$$\psi = \psi_s + \epsilon\psi_u, \quad \phi = \epsilon\phi_u, \quad R = 1 + W\zeta_s + \epsilon\zeta_u, \tag{8}$$

where the subscripts s and u denote the steady and unsteady solutions respectively. In (8), note that there is no steady fluid motion because no shear stress is exerted by the electric field at the drop surface in the perfectly conducting limit (see Melcher & Taylor 1969). The steady-state solutions that are sufficient for the present purpose are (see Feng 1990)

$$\psi_s = \left(r - \frac{1}{r^2}\right) P_1(\eta) + O(W), \quad \zeta_s = \tfrac{3}{4} P_2(\eta) + O(W), \tag{9}$$

where η is defined as $\eta = \cos\theta$ for convenience. Then the governing equations for the unsteady parts are

$$\nabla^2 \psi_u = 0 \quad \text{and} \quad \nabla^2 \phi_u = 0. \tag{10}$$

Here, we use the standard domain perturbation technique to transform the boundary conditions at $r = 1 + W\zeta_s + \epsilon\zeta_u$ to the equivalent boundary conditions at $r = 1$. Then the equivalent boundary conditions for the unsteady motion are

$$\nabla \psi_u \to 0 \quad \text{as} \quad r \to \infty, \tag{11}$$

and at $r = 1$, we have

(i) kinematic condition:

$$\frac{\partial \zeta_u}{\partial t} = \frac{\partial \phi_u}{\partial r} + W\left(\zeta_s \frac{\partial^2 \phi_u}{\partial r^2} - \frac{\partial \zeta_s}{\partial \theta}\frac{\partial \phi_u}{\partial \theta}\right), \tag{12}$$

(ii) normal stress condition:

$$W\left(\frac{\partial \psi_s}{\partial r}\right)\left(\zeta_u \frac{\partial^2 \psi_s}{\partial r^2} + \frac{\partial \psi_u}{\partial r} - \frac{\partial \zeta_u}{\partial \theta}\frac{\partial \psi_s}{\partial \theta}\right) - \frac{\partial \phi_u}{\partial t} - W\zeta_s \frac{\partial^2 \phi_u}{\partial r \partial t} + \frac{1}{\epsilon}\left[-2S\epsilon \frac{\partial^2 \phi_u}{\partial \hat{n}^2} + p_v\right] = \frac{1}{\epsilon}[(\nabla \cdot \hat{\boldsymbol{n}}) - (\nabla \cdot \hat{\boldsymbol{n}})_s], \tag{13}$$

(iii) infinite-permittivity condition:

$$\psi_u + \zeta_u \frac{\partial \psi_s}{\partial r} + O(W) = 0, \tag{14}$$

where all terms are evaluated at $r = 1$ except for those in square brackets in (13). These terms, $-2S(\partial^2 \phi_u / \partial \hat{n}^2)$, p_v, and $\nabla \cdot \hat{\boldsymbol{n}}$, should be evaluated at $R = 1 + W\zeta_s + \epsilon\zeta_u$, while $(\nabla \cdot \hat{\boldsymbol{n}})_s$ at $R_s = 1 + W\zeta_s$. As we see in (14), the infinite-permittivity condition imposes a relation between ψ_u and ζ_u. But ψ_u appears only in the first term of the normal stress condition, which is $O(W)$. Therefore, the infinite-permittivity condition up to $O(1)$ terms is sufficient for the present purpose.

Now, we assume that the solution can be expanded for the unsteady parts in the forms

$$\zeta_u = \sum_{n=0}^{\infty} \alpha_n(t) P_n(\eta), \quad \phi_u = \sum_{n=0}^{\infty} \beta_n(t) r^n P_n(\eta), \quad \psi_u = \sum_{n=0}^{\infty} \gamma_n(t) r^{-(n+1)} P_n(\eta). \tag{15}$$

Then the curvature term in (13) is given as (see Kang & Leal 1988)

$$\frac{1}{\epsilon}[(\nabla \cdot \hat{\boldsymbol{n}}) - (\nabla \cdot \hat{\boldsymbol{n}})_s] = \sum_{n=0}^{\infty} \alpha_n (n+2)(n-1) P_n(\eta) - 2W\left(\sum \alpha_n P_n \sum b_k^{(s)} (k^2 + k - 1) P_k + \sum b_k^{(s)} P_k \sum \alpha_n (n^2 + n - 1) P_n\right) + O(W^2), \tag{16}$$

where $b_k^{(s)}$ are the coefficients in $\zeta_s = \sum_{k=0}^{\infty} b_k^{(s)} P_n(\eta)$ for the steady-state shape function in (9).

Now we consider the viscous pressure correction term, p_v. As mentioned earlier, the viscous pressure correction should be evaluated at $r = 1 + W\zeta_s + \epsilon\zeta_u$. Unfortunately, however, the domain perturbation technique may not be used for the term because of the singular nature of p_v at the drop surface when $S \to 0$. In other words, there exists a boundary layer near the drop surface, and thus the domain perturbation technique does not work for this case. However, the viscous pressure correction at the drop surface should be a continuous and smooth function of the drop shape. Thus, we may still use the approximation

$$p_v(1 + W\zeta_s + \epsilon\zeta_u, \theta) = p_v^*(1, \theta) + (W\zeta_s + \epsilon\zeta_u)\, O(p_v^*(1, \theta)) \tag{17}$$

where $p_v^*(1, \theta)$ denotes the viscous pressure correction if the drop had assumed a spherical shape. As will be shown shortly, the viscous pressure correction due to the $O(\epsilon)$ unsteady fluid motion is $O(\epsilon S)$. Thus, the error in approximation (17) is at most $O(\epsilon SW)$ or $O(\epsilon^2 S)$. Thus, the terms of $O(\epsilon SW)$ or $O(\epsilon^2 S)$ can be neglected compared with those of $O(\epsilon W)$, $O(\epsilon S)$ or larger.

Now, we decompose the velocity field into the potential flow field and the disturbance field due to the viscosity effect as

$$\boldsymbol{u} = \boldsymbol{u}_p + \boldsymbol{u}_v;$$

then for the $O(\epsilon)$ flow fields, $\boldsymbol{u}_v$ is $O(\epsilon)$ or smaller. Thus, the Navier–Stokes equation for the weak viscous correction (i.e. $S \ll 1$) in dimensionless form is given as

$$\frac{\partial \boldsymbol{u}_v}{\partial t} = -\nabla p_v + S\nabla^2 \boldsymbol{u}_v. \tag{18}$$

The vorticity equation corresponding to (18) is

$$\frac{\partial \boldsymbol{\omega}}{\partial t} = -S\nabla \times (\nabla \times \boldsymbol{\omega}), \tag{19}$$

where $\boldsymbol{\omega} = \nabla \times \boldsymbol{u}_v$.

For an axisymmetric problem, the vorticity can be expressed with the toroidal field as (see Prosperetti 1977 and Kang & Leal 1988)

$$\boldsymbol{\omega} = \sum_{n=0}^{\infty} \nabla \times (T_n(r)\, P_n(\cos\theta)\, \boldsymbol{e}_r). \tag{20}$$

Then, as shown by Prosperetti (1977),

$$p_v^*(1, \theta) = -\sum_{n=0}^{\infty} (n+1)\, S T_n(1)\, P_n(\cos\theta). \tag{21}$$

From (20) and the definition of vorticity, we may show that

$$\omega = -\sum_{n=0}^{\infty} \frac{T_n(r)}{r} \frac{\mathrm{d}P_n}{\mathrm{d}\theta} = \frac{\partial u_\theta}{\partial r} + \frac{u_\theta}{r} - \frac{1}{r}\frac{\partial u_r}{\partial \theta}. \tag{22}$$

For a perfectly conducting drop, the tangential stress must vanish at $r = 1$, i.e.

$$\frac{\partial u_\theta}{\partial r} - \frac{u_\theta}{r} + \frac{1}{r}\frac{\partial u_r}{\partial \theta} = 0. \tag{23}$$

By eliminating $\partial u_\theta/\partial r$ in (22) by using (23), we have

$$-\sum_{n=0}^{\infty}\frac{T_n(1)}{r}\frac{\mathrm{d}P_n}{\mathrm{d}\theta}=2\left(\frac{u_\theta}{r}-\frac{1}{r}\frac{\partial u_r}{\partial\theta}\right)\approx 2\left(\frac{u_{p\theta}}{r}-\frac{1}{r}\frac{\partial u_{pr}}{\partial\theta}\right), \tag{24}$$

where the approximation $\boldsymbol{u}=\boldsymbol{u}_p+o(1)\,O(\|\boldsymbol{u}_p\|)$ for $S\to 0$ has been used. Differently from the no-slip boundary case, the potential flow solution is a true limiting solution as $S\to 0$ in the free-surface problems, where the shear stress vanishes. Furthermore the $O(\epsilon)$ solution for $T_n(1)$ is sufficient for the present purpose because p_v^* is $O(\epsilon S)$ as we can see from (21).

In the above, we have seen how the vorticity is generated at the curved drop surface due to the vanishing tangential stress condition and how the pressure is affected by the vorticity generated at the surface. For the present problem, the potential flow field is given as

$$\boldsymbol{u}_p=\epsilon\nabla\phi_u,\quad \phi_u=\sum_{n=0}^{\infty}\beta_n r^n P_n(\eta). \tag{25}$$

By substituting (25) into (24), we have

$$T_n(1)=2\epsilon\beta_n(n-1). \tag{26}$$

Therefore, from (21) and (26),

$$p_v^*(1,\theta)=-\epsilon\sum_{n=0}^{\infty}(2S)\,\beta_n(n-1)\,(n+1)\,P_n(\cos\theta). \tag{27}$$

On the other hand, the viscous normal stress is given as

$$-(2S)\frac{\partial^2\phi}{\partial\hat{n}^2}\bigg|_{r=1}=-\epsilon\sum_{n=0}^{\infty}(2S)\,\beta_n(n-1)\,nP_n(\cos\theta). \tag{28}$$

Here, we must note that both $p_v^*(1,\theta)$ and $-2S(\partial^2\phi/\partial\hat{n}^2)$ are $O(\epsilon S)$, but $|p_v^*(1,\theta)|>|-2S(\partial^2\phi/\partial\hat{n}^2)|$ for all n. This fact means that the viscous pressure correction is no less important than the viscous normal stress, and we should include the viscous pressure correction whenever we consider the viscosity effect.

One important point that we should note is that the viscous pressure correction and the viscous normal stress exert forces on the drop surface in the opposite direction to the surface motion and consequently act as damping stresses. This point becomes obvious if we see the contributions from each mode. For the nth mode,

$$u_{pr}(1,\theta)=\epsilon\frac{\partial\phi_u}{\partial r}\bigg|_{r=1}=\epsilon n\beta_n P_n(\eta),$$

$$-(2S)\frac{\partial^2\phi}{\partial\hat{n}^2}+p_v^*=-\epsilon(2S)\,(n-1)\,(2n+1)\,\beta_n P_n(\eta).$$

Along this line of discussion, one related work is worthy of note. Feng & Beard (1991*a*) defined the viscous damping stress N_d as $N_d=p_v+(-2S)\,\partial^2\phi/\partial\hat{n}^2$ in our notation and obtained N_d in an *indirect* way. They could get the same result as in this work by equating the rate of overall work done by N_d to the total rate of dissipation of mechanical energy for each mode. Thus, it is clearly shown that the approach in the present work is completely equivalent to those based on the dissipation theory.

By using the information in (16), (27), and (28), the normal stress condition can be expressed as

$$W\left(\frac{\partial\psi_s}{\partial r}\right)\left(\zeta_u\frac{\partial^2\psi_s}{\partial r^2}+\frac{\partial\psi_u}{\partial r}-\frac{\partial\zeta_u}{\partial\theta}\frac{\partial\psi_s}{\partial\theta}\right)-\frac{\partial\phi_u}{\partial t}-W\zeta_s\frac{\partial^2\phi_u}{\partial r\partial t}-\sum_{n=0}^{\infty}(2S)\beta_n(n-1)(2n+1)P_n$$
$$=\sum\alpha_n(n+2)(n-1)P_n-2W\sum\alpha_nP_n\sum b_k^{(s)}(k^2+k-1)P_k$$
$$-2W\sum b_k^{(s)}P_k\sum\alpha_n(n^2+n-1)P_n+O(SW)+O(W^2). \tag{29}$$

Now, it is straightforward to proceed. First, the expansions for steady and unsteady solutions ((9) and (15)) are substituted into the kinetmatic condition (12), the normal stress condition (29), and the infinite permittivity condition (14). Then we simplify the equations by using the well-known formulae for the products of the Legendre polynomials. The detailed procedure is very similar to those in Kang & Leal (1988) and Feng (1990). The kinematic condition is then expressed in the form

$$\dot{\alpha}_n=WH_{+2}(n)\beta_{n+2}+(n+WH_0(n))\beta_n+WH_{-2}(n)\beta_{n-2}, \tag{30}$$

and the normal stress condition and the infinite permittivity condition are combined to be expressed as

$$-\dot{\beta}_n(1+WB_0(n))-WB_{+2}(n)\dot{\beta}_{n+2}-WB_{-2}(n)\dot{\beta}_{n-2}-2S(n-1)(2n+1)\beta_n$$
$$=((n+2)(n-1)+WC_0(n))\alpha_n+WC_{+2}(n)\alpha_{n+2}+WC_{-2}(n)\alpha_{n-2}, \tag{31}$$

where $H_i(n)$, $B_i(n)$, and $C_i(n)$ are rational functions of n, detailed expressions for which are not given here. From (30) and (31), β_n, $\beta_{n\pm2}$, $\dot{\beta}_n$, and $\dot{\beta}_{n\pm2}$ are eliminated to obtain

$$\ddot{\alpha}_n+2S(n-1)(2n+1)\dot{\alpha}_n+(n-1)n(n+2)(1-WA_0(n))\alpha_n$$
$$=-WA_{+2}(n)\alpha_{n+2}-WA_{-2}(n)\alpha_{n-2}+O(SW)+O(W^2), \tag{32}$$

where
$$A_0(n)=\frac{9(2n^5+23n^4+21n^3-17n^2-7n-2)}{4(2n-1)(2n+1)(2n+3)(n-1)(n+2)}$$

and $A_{\pm2}(n)$ are the rational functions of n, precise expressions for which we do not need for the present purpose.

As a special case of (32), we have for $W=0$

$$\ddot{\alpha}_n+2S(n-1)(2n+1)\dot{\alpha}_n+(n-1)n(n+2)\alpha_n=0, \tag{33}$$

which is the famous result obtained earlier by Lamb (1932) via the theory of viscous dissipation. Let us now consider the frequency modification and the damping coefficient in the case of non-zero W. To do that we define

$$\alpha_n=\mathrm{e}^{-S(n-1)(2n+1)t}\tilde{\alpha}_n\equiv\mathrm{e}^{-\frac{t}{\tau_n}}\tilde{\alpha}_n, \tag{34}$$

where $\tilde{\alpha}_n$ is expected to exhibit purely oscillatory behaviour at least up to $O(W)$. Then (32) becomes

$$\ddot{\tilde{\alpha}}_n+(n-1)n(n+2)(1-WA_0(n)-S^2D_0(n))\tilde{\alpha}_n$$
$$=-WA_{+2}(n)O(1)\tilde{\alpha}_{n+2}-WA_{-2}(n)O(1)\tilde{\alpha}_{n-2}+O(SW)+O(W^2), \tag{35}$$

where
$$D_0(n)=\frac{(n-1)(2n+1)^2}{n(n+2)}$$

and $O(1)$ means an $O(1)$ term as both W and $S\to0$. Now we assume that for each mode

$$\tilde{\alpha}_n=\tilde{\alpha}_{n0}\mathrm{e}^{\mathrm{i}\omega t}. \tag{36}$$

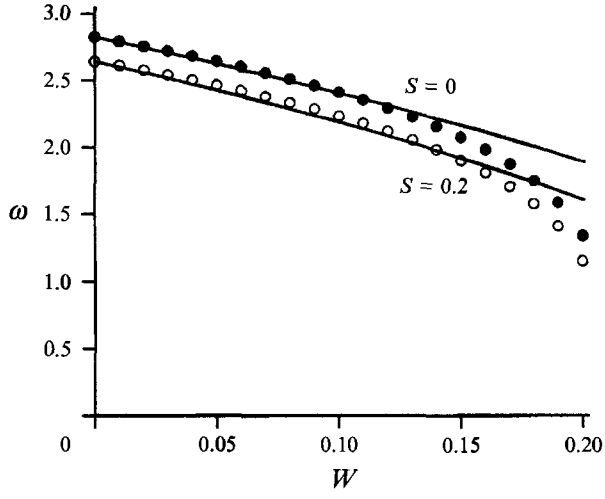

FIGURE 2. Frequency modification as a function of W and S (solid lines: predictions by equation (37) for the $n = 2$ mode, symbols: predictions from the analysis based on the spheroidal approximation).

Then (36) can be expressed compactly as

$$\boldsymbol{A}\boldsymbol{x} = \boldsymbol{0},$$

where $\boldsymbol{A}$ is a tridiagonal matrix with

$$\begin{aligned} a_{n,n} &= \omega^2 - (n-1)\,n(n+2)\,(1 - WA_0(n) - S^2 D_0(n)), \\ a_{n,n+1} &= WA_{+2}(n)\,O(1), \\ a_{n,n-1} &= WA_{-2}(n)\,O(1), \end{aligned}$$

and $x = (\tilde{\alpha}_{20}, \tilde{\alpha}_{30}, \ldots)^T$. As well known, the oscillation frequency is determined from the condition

$$\det(\boldsymbol{A}) = 0.$$

Here, we should note that any off-diagonal element must be multiplied by another off-diagonal element in a computation of the determinant of $\boldsymbol{A}$. In other words, off-diagonal elements can contribute to the determinant by at most $O(W^2)$. Therefore, there is no mode–mode interaction up to $O(W)$, and the nth mode oscillation frequency, ω_n, can be predicted from $a_{n,n} = 0$. The final result is

$$\begin{aligned} \frac{\omega_n^2}{\omega_{n0}^2} &= 1 - A_0(n)\,W - D_0(n)\,S^2 \\ &= 1 - \frac{9(2n^5+23n^4+21n^3-17n^2-7n-2)}{4(2n-1)(2n+1)(2n+3)(n-1)(n+2)}\,W - \frac{(n-1)(2n+1)^2}{n(n+2)}\,S^2, \end{aligned} \tag{37}$$

where ω_{n0}^2 is the square of the frequency of the nth mode for the case of no electric field and no viscosity defined in (7).

When $S = 0$, (37) reduces to Feng's asymptotic formula for the frequency modification (equation (7)). In figure 2, the oscillation frequencies for the $n = 2$ mode predicted from (37) (solid lines) are compared with the results obtained via the spheroidal approximation (closed and open circles). Closed circles ($S = 0$ case) correspond to the result obtained earlier by Brazier-Smith *et al.* In later part of the present work (§5), the theory of Brazier-Smith *et al.* is extended to include the weak

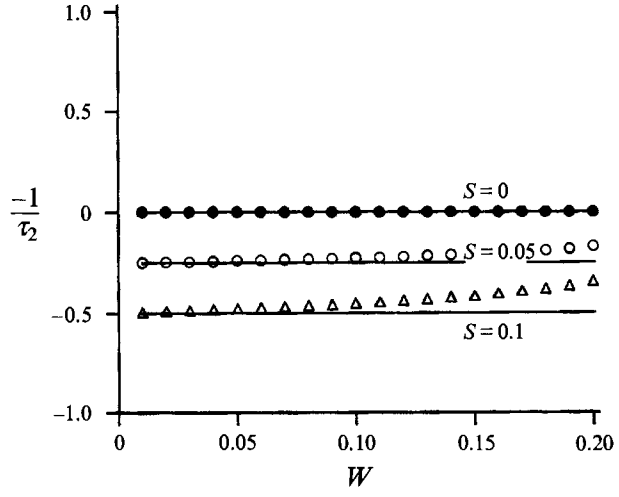

FIGURE 3. Damping factor as a function of W and S (solid lines: predictions by equation (34) for the $n = 2$ mode; symbols: predictions from the analysis based on the spheroidal approximation).

viscous effect. Open circles are for the frequency change predicted by the extended theory in §5. As we can see, the agreement is very good for small W and S values. The damping coefficient predicted by the two different approximations are compared in figure 3. The solid lines correspond to the result for the $n = 2$ mode from (34) and the symbols correspond to the prediction by the extended theory based on the spheroidal approximation. The agreement between the results is excellent when both S and W are small. However, for a given S value, the two results deviate from each other as W increases. The discrepancy may be explained by the following two facts. First, the deformed shape by the P_2-mode is spheroidal only when the deformation is small. Second, the terms of $O(SW)$ are neglected in the perturbation analysis.

3.2. *Decomposition of frequency change into two parts*

Formula (37) gives the frequency modification due to a steady electric field. It is well known that if the equilibrium shape of the drop is deformed away from a sphere by a steady force, the frequency changes too no matter what the causes are. Hence it is desirable to separate the frequency change due to the electric field $(-A_0(n)\,W)$ into two parts: (i) one caused by the special effect of the electric field $(-A_{01}(n)\,W)$ and (ii) the other caused by a change in equilibrium shape $(-A_{02}(n)\,W)$. It is easy to show that the two separate effects are linearly additive up to $O(W)$ as

$$\left.\frac{\omega_n^2}{\omega_{n0}^2}\right|_{S=0} = 1 - A_0(n)\,W = 1 - A_{01}(n)\,W - A_{02}(n)\,W. \tag{38}$$

The frequency change due to the special effect of the electric field $(-A_{01}(n)\,W)$ can be easily obtained by considering only the oscillation about spherical shape ((i.e. by setting $\zeta_s = 0$ and $S = 0$ in the boundary conditions (12)–(14)). In this case, the appropriate boundary conditions reduce to

(i) kinematic condtiion:

$$\frac{\partial \zeta_u}{\partial t} = \frac{\partial \phi_u}{\partial r}, \tag{39}$$

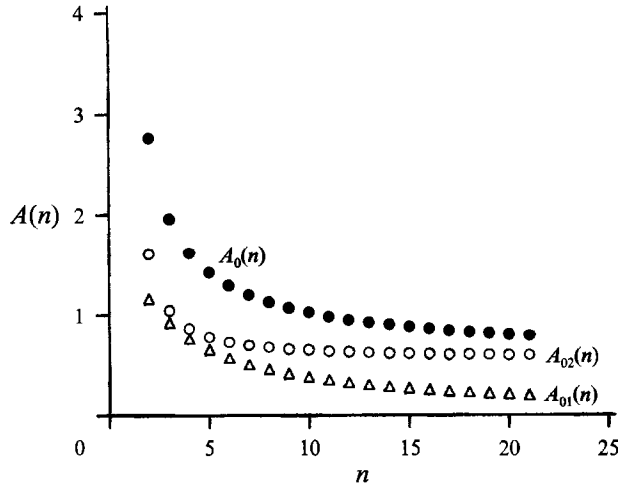

FIGURE 4. Frequency change coefficients as functions of n.

(ii) normal stress condition:

$$W\left(\frac{\partial \psi_s}{\partial r}\right)\left(\zeta_u \frac{\partial^2 \psi_s}{\partial r^2}+\frac{\partial \psi_u}{\partial r}-\frac{\partial \zeta_u}{\partial \theta}\frac{\partial \psi_s}{\partial \theta}\right)-\frac{\partial \phi_u}{\partial t}=\sum_{n=0}^{\infty}\alpha_n(n+2)(n-1)P_n(\eta), \tag{40}$$

(iii) infinite-permittivity condition:

$$\psi_u+\zeta_u\frac{\partial \psi_s}{\partial r}=0. \tag{41}$$

The analysis is simple and only the final result is given here:

$$A_{01}(n)=\frac{9n(4n^3+2n^2-6n-1)}{(2n-1)(2n+1)(2n+3)(n-1)(n+2)}. \tag{42}$$

Hence the effect due to the non-spherical equilibrium shape is obtained from $A_{02}(n)=A_0(n)-A_{01}(n)$ as

$$A_{02}(n)=\frac{9(n+1)(n^3+2n^2+3n-2)}{4(2n-1)(2n+3)(n-1)(n+2)}. \tag{43}$$

In the above, we have seen that the frequency modification due to the deformed equilibrium shape $R_s(\eta)=1+\frac{3}{4}WP_2(\eta)$ is given by $\omega_n^2/\omega_{n0}^2=1-A_{02}(n)W$ (no matter what the causes are) as long as there is no fluid motion at the equilibrium state. Of course, in the present problem, $W\geqslant 0$ and only prolate or spherical equilibrium shapes are possible. However, for certain problems due to other forces of deformation, oblate equilibrium shapes may also be possible. In that situation, the result (43) suggests that the frequency of oscillation may increase if the equilibrium shape is oblate and there is no fluid motion at equilibrium. In analogy to the problem of a vibrating string, the tendency of frequency change due to deformed equilibrium shape may possibly be explained in terms of the circumferential arclength of the section of drop along the rotation axis. When the equilibrium shape is given as $R_s(\eta)=1+\epsilon P_2(\eta)$, the circumferential arclength is $2\pi(1+\frac{1}{4}\epsilon)+O(\epsilon^2)$. Thus, for a prolate shape it is longer than for the sphere case, but it is shorter for an oblate shape, at least up to $O(\epsilon)$.

In figure 4, the two separate contributions ($A_{01}(n)$ and $A_{02}(n)$) are plotted as functions of n along with the total frequency change coefficient ($A_0(n)$). As we can see,

two effects show different asymptotic behaviour as $n \to \infty$. The special effect of the electric field diminishes ($A_{01}(n) \to 0$ as $n \to \infty$), while the effect of deformed equilibrium shape persists ($A_{02}(n) \to \frac{9}{16}$ as $n \to \infty$). The persisting nature of $A_{02}(n)$ may also be understood by the change in circumferential arclength as mentioned above.

4. Derivation of a dynamical equation based on the spheroidal approximation

Thus far, as a preliminary, we have studied the results from the perturbation analysis for the frequency modification due to a steady electric field in the limit $0 \leqslant W \ll 1$ and $0 \leqslant S \ll 1$. Now we are in a position to start the main part of the present work on the dynamic response of a conducting drop to a time-periodic electric field. Differently from the preceding section, hereafter we perform a global analysis to study the nonlinear dynamical behaviour, such as two-timing oscillation and indefinite stretching after chaotic oscillation, exhibited by a drop in a time-periodic electric field. However, as mentioned earlier, several results in the preceding section will be used in the global analysis.

For the purpose of our global analysis, the most desirable analytical approach is, of course, a rigorous solution of the full problem, but that is not practical. On the other hand, one can solve the exact problem numerically over a considerable range of the parameter space. However, the limitation of a purely numerical approach is the necessity of solving a very large number of special cases to obtain a general understanding. Thus, we consider a dynamical model to explore the characteristics of the drop response to a time-periodic electric field.

We first derive a reasonably simple dynamical equation in the form of an ordinary differential equation for a drop in an arbitrary time-dependent, uniform electric field. To derive the dynamical equation, we extend the analyses of Taylor (1964) and Brazier-Smith *et al.* (1971) and assume that the drop takes a spheroidal shape at any time as shown in figure 5. Let us start the derivation with a geometrical consideration of a spheroidal drop. In figure 5, the x-axis is the symmetric axis, and $a(t)$ and $b(t)$ are dimensionless radii on the x-axis and σ-axis respectively. The volume conservation relation now is

$$ab^2 = 1, \tag{44}$$

from which we have the relation

$$\frac{\dot{a}}{2a} = -\frac{\dot{b}}{b}. \tag{45}$$

Now we want to derive a dynamical equation in terms of $a(t)$ by considering the normal stress condition

$$\tfrac{1}{2}W(t)\left(\frac{\partial\psi}{\partial\hat{n}}\right)^2 - \frac{\partial\phi}{\partial t} - \tfrac{1}{2}\nabla\phi\cdot\nabla\phi - 2S\frac{\partial^2\phi}{\partial\hat{n}^2} + p_v + G(t) = \nabla\cdot\hat{\boldsymbol{n}}. \tag{46}$$

In the following subsections each term in (46) will be expressed in terms of $a(t)$ under the spheroidal approximation.

4.1. *Velocity potential inside the drop*

For the coordinate system in figure 5, the Laplace equation has the form

$$\nabla^2\phi = \frac{1}{\sigma}\frac{\partial}{\partial\sigma}\left(\sigma\frac{\partial\phi}{\partial\sigma}\right) + \frac{\partial^2\phi}{\partial x^2} = 0. \tag{47}$$

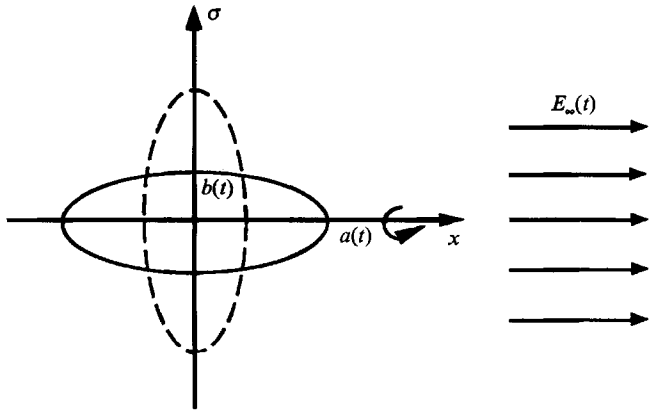

FIGURE 5. A spheroidal conducting drop in a time-dependent electric field.

The solution of the Laplace equation inside the spheroidal drop can be written as (Brazier-Smith *et al.* 1971)

$$\phi = -\tfrac{1}{2}B(t)\,\sigma^2 + B(t)\,x^2, \tag{48}$$

where $B(t)$ is a function of time only. By applying the kinematic condition at the poles (or the equator) $(\partial\phi/\partial x)|_{x=a} = 2Ba = \dot{a}$, we have

$$B(t) = \frac{\dot{a}}{2a}.$$

Here, we must note that the solution (48) with $B(t) = \dot{a}/2a$ satisfies the kinematic condition at all points on the drop surface. The shape function for a spheroidal shape is given as

$$F = \frac{x^2}{a^2} + \frac{\sigma^2}{b^2} - 1 = 0. \tag{49}$$

Then
$$-\frac{1}{|\nabla F|}\frac{\partial F}{\partial t} = \frac{((\dot{a}/a^3)\,x^2 - (\dot{a}/2ab^2)\,\sigma^2)}{((x^2/a^4) + (\sigma^2/b^4))^{\frac{1}{2}}}.$$

On the other hand
$$\hat{n} = \frac{\nabla F}{|\nabla F|} = \frac{(x/a^2, \sigma/b^2)}{((x^2/a^4) + (\sigma^2/b^4))^{\frac{1}{2}}}$$

and
$$\nabla\phi = (2Bx, -B\sigma) = ((\dot{a}/a)\,x, -(\dot{a}/2a)\,\sigma).$$

Thus, the kinematic condition (4) is satisfied at all points on the boundary. Therefore

$$\phi = \frac{\dot{a}}{2a}x^2 - \frac{\dot{a}}{4a}\sigma^2 \tag{50}$$

is a complete solution for the velocity potential inside the drop. Now, we may express the values of several terms in (46) at poles and equators in terms of $a(t)$ for later use as

$$\left.\frac{\partial\phi}{\partial t}\right|_{x=a} = \tfrac{1}{2}(a\ddot{a} - \dot{a}^2), \quad \left.\frac{\partial\phi}{\partial t}\right|_{\sigma=b} = -\frac{1}{4a^3}(a\ddot{a} - \dot{a}^2),$$

$$\nabla\phi\cdot\nabla\phi|_{x=a} = \dot{a}^2, \quad \nabla\phi\cdot\nabla\phi|_{\sigma=b} = \dot{a}^2/4a^3.$$

4.2. *Electric potential outside the spheroid*

The potential distribution outside a conducting spheroidal drop is given in Landau & Lifshitz (1975), and the normal component of the electric field can be easily obtained as the following (for an prolate drop, it is given in Taylor 1964).

(i) Prolate drop ($a > b$):

$$\frac{\partial \psi}{\partial \hat{n}} = \frac{xP}{b^2 I_2} = \frac{axP}{I_2}, \tag{51}$$

where $$P = \frac{1}{(a-(e^2x^2/a))^{\frac{1}{2}}}, \quad I_2 = \frac{1}{2e^3}\ln\left(\frac{1+e}{1-e}\right) - \frac{1}{e^2}, \quad e = \left(1-\frac{1}{a^3}\right)^{\frac{1}{2}}.$$

(ii) Oblate drop ($b > a$):

$$\frac{\partial \psi}{\partial \hat{n}} = \frac{xQ}{b^2 I_3} = \frac{axQ}{I_3}, \tag{52}$$

where $$Q = \frac{1}{(a+(\tilde{e}^2x^2/a))^{\frac{1}{2}}}, \quad I_3 = \frac{\tilde{e}-\tan^{-1}\tilde{e}}{\tilde{e}^3}, \quad \tilde{e} = \left(\frac{1}{a^3}-1\right)^{\frac{1}{2}}.$$

At poles ($x = \pm a$), $P = Q = a$, and the expression for $\partial\psi/\partial\hat{n}$ reduces to

$$\frac{\partial \psi}{\partial \hat{n}} = \pm\frac{a^3}{I_2} \text{ for a prolate drop,}$$

$$\frac{\partial \psi}{\partial \hat{n}} = \pm\frac{a^3}{I_3} \text{ for an oblate drop.}$$

4.3. *Curvature terms*

The expression for the curvature may be easily obtained from

$$\nabla\cdot\hat{n} = \frac{\partial \hat{n}_x}{\partial x} + \frac{1}{\sigma}\frac{\partial(\sigma \hat{n}_\sigma)}{\partial \sigma}. \tag{53}$$

After evaluating $(\nabla\cdot\hat{n})$ at the poles and the equator, we have

$$\nabla\cdot\hat{n}|_{x=1} = 2a^2, \quad \nabla\cdot\hat{n}|_{\sigma=b} = \frac{1}{a^{\frac{5}{2}}} + a^{\frac{1}{2}}. \tag{54a, b}$$

4.4. *Weak viscous effect*

Since information on the viscous pressure corretion is not available, we borrow the result for the near-sphere oscillation that was obtained in §3. As shown earlier for the velocity potential

$$\phi = \epsilon \sum \beta_n r^n P_n(\cos\theta), \tag{55}$$

the pressure correction is given by

$$p_v = -2S\sum(\epsilon\beta_n)(n-1)(n+1)P_n(\cos\theta). \tag{56}$$

In spheroidal motion,

$$\phi = -\tfrac{1}{2}B\sigma^2 + Bx^2; \quad B = \dot{a}/2a. \tag{57}$$

By taking $x = r\cos\theta$, $\sigma = r\sin\theta$, ϕ is reduced to

$$\phi = Br^2 P_2(\cos\theta). \tag{58}$$

Therefore, $\epsilon\beta_2 = B = \dot{a}/2a$, $\beta_n = 0$ if $n \neq 2$. Thus the viscous pressure correction may be approximated by

$$p_v = -6S(\dot{a}/2a)\,P_2(\cos\theta),$$

and at the poles ($x = \pm a$):

$$p_v = -3S\dot{a}/a, \tag{59a}$$

and at the equatorial plane ($\sigma = b$):

$$p_v = \tfrac{3}{2}S\dot{a}/a. \tag{59b}$$

The expression for $-2S(\partial^2\phi/\partial\hat{n}^2)$ can also be obtained from (57), and it has at the poles

$$-2S\frac{\partial^2\phi}{\partial\hat{n}^2} = -2S\frac{\dot{a}}{a}, \tag{60a}$$

and at the equatorial plane

$$-2S\frac{\partial^2\phi}{\partial\hat{n}^2} = S\frac{\dot{a}}{a}. \tag{60b}$$

Comparing (59) with (60) we see that

$$p_v = \frac{3}{2}\left(-2S\frac{\partial^2\phi}{\partial\hat{n}^2}\right)$$

at both the poles and the equatorial plane, and this is consistent with the findings for the small-deformation case in the preceding section.

As shown above, the weak viscous effect has been derived based on the near-sphere oscillation. However, it will be shown later in this section that the results in (59) and (60) are equally valid for an arbitrary degree of deformation as far as the spheroidal approximation is used. In §4.6, the weak viscous effect will be reanalysed using the dissipation theory.

4.5. *Dynamical equation in terms of $a(t)$*

We put all the information obtained so far into the normal stress condition, and obtain the following results. At the poles ($x = \pm a, \sigma = 0$)

$$\tfrac{1}{2}W(t)\left(\frac{\partial\psi}{\partial\hat{n}}\right)^2_{pole} - \tfrac{1}{2}(a\ddot{a} - \dot{a}^2) - \tfrac{1}{2}\dot{a}^2 - 5S\dot{a}/a + G(t) = 2a^2, \tag{61a}$$

and at the equatorial plane ($x = 0, \sigma = b$)

$$0 + \frac{1}{4a^3}(a\ddot{a} - \dot{a}^2) - \frac{1}{8}\frac{\dot{a}^2}{a^3} + \frac{5}{2}S\frac{\dot{a}}{a} + G(t) = \frac{1}{a^5} + a^{\frac{1}{2}}. \tag{61b}$$

By eliminating $G(t)$ from (61 a) and (61 b), we finally obtain an equation for the drop dynamics in an electric field in terms of $a(t)$:

$$\ddot{a} = \frac{4a^2}{2a^3+1}\left[\tfrac{1}{2}W(t)\,E^2_{n,\,pole} + \frac{3}{8}\frac{\dot{a}^2}{a^3} - \frac{15}{2}S\frac{\dot{a}}{a} - 2a^2 + \frac{1}{a^5} + a^{\frac{1}{2}}\right], \tag{62}$$

where $E^2_{n,\,pole} = (\partial\psi/\partial\hat{n})^2_{pole}$ has the following expressions depending on whether $a > 1$ or $a < 1$:

$$E^2_{n,\,pole} = (a^3/I_2)^2 \quad \text{if} \quad a > 1, \tag{63a}$$

$$E^2_{n,\,pole} = (a^3/I_3)^2 \quad \text{if} \quad a < 1. \tag{63b}$$

In (63), I_2 and I_3 are the functions of $a(t)$ defined in (51) and (52).

The dynamical equation (62) is the most important result of the present paper. In the following sections, we will discuss the results predicted from (62) after briefly reanalysing the weak viscous effect.

4.6. *Weak viscous effect via the dissipation theory*

The weak viscous effect may also be predicted by the dissipation theory. The energy conservation law for the whole drop is given by

$$\frac{\mathrm{d}}{\mathrm{d}t}(K+P) = -D, \tag{64}$$

where K and P are the kinetic and potential energies and D is the viscous dissipation. When the velocity of the fluid is given by (50), the kinetic energy may be easily obtained as

$$K = \frac{1}{2}\int \nabla\phi\cdot\nabla\phi \,\mathrm{d}V = \frac{\pi}{15}\left(\frac{\dot{a}}{a}\right)^2\left(2a^2+\frac{1}{a}\right), \tag{65}$$

where we have used the relation $ab^2 = 1$ to eliminate b. On the other hand, the dimensionless viscous dissipation may be obtained from the surface integral when the flow field is given by the potential flow field as (see Batchelor 1967)

$$D = S\int \frac{\partial}{\partial n}(\nabla\phi\cdot\nabla\phi)\,\mathrm{d}A,$$

where S is the dimensionless number defined earlier in §2. By using the velocity potential function in (50), we may show that

$$D = 4\pi(\dot{a}/a)^2 S. \tag{66}$$

Now, by substituting (65) and (66) into (64), we may show that

$$\ddot{a} = \frac{4a^2}{2a^3+1}\left[\frac{3}{8}\frac{\dot{a}^2}{a^3} - \frac{15}{2}S\frac{\dot{a}}{a} + \dots\right], \tag{67}$$

where other terms are from the potential energy contribution due to the electric field and surface tension. By comparing (62) and (67), we may see that exactly the same predictions are obtained from both approaches.

5. Dynamics of a drop in a steady electric field

Earlier, in §3, we discussed the results for the dynamics of a drop in a steady electric field that were obtained by the perturbation analysis. In this section, we discuss the dynamical behaviour in a steady field that is predicted by the dynamical model equation (62). For steady electric field, $W(t) = W =$ constant, and the steady-state solution of the dynamical equation is obtained from

$$\tfrac{1}{2}W E^2_{n,\,pole} = 2a^2 - \frac{1}{a^{\frac{5}{2}}} - a^{\frac{1}{2}}. \tag{68}$$

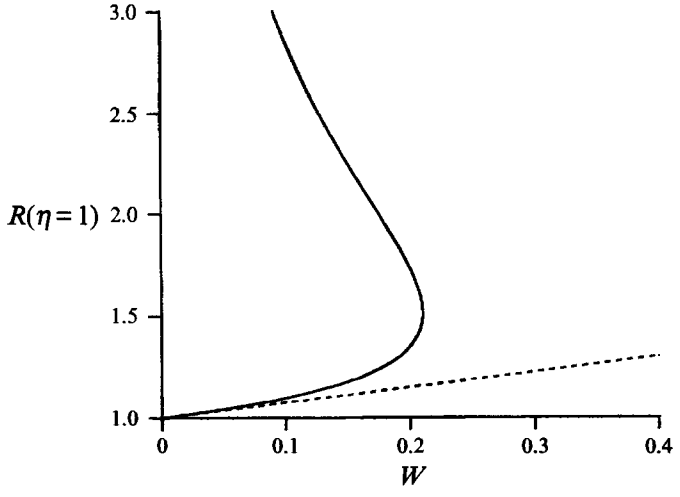

FIGURE 6. Comparison of Taylor's solution with perturbation solution (solid line: Taylor's solution; dotted line: the first-order perturbation solution).

The solution of (68) is identical to Taylor's result and is given in figure 6, where the first-order perturbation solution is also given for comparison (see (9) for the perturbation solution). As shown in figure 6, there is a limiting value of W for the existence of a steady-state solution. The limiting value of W is termed the critical Weber number and denoted by W_c. Thus, the steady-state solution has two branches of stable and unstable solutions. Taylor's result has been verified by exact numerical solutions (Basaran & Scriven 1989; Miksis 1981). Basaran & Scriven used the finite-element method and Miksis used the boundary-integral technique to solve the problem. The numerical solutions showed that Taylor's solution is surprisingly accurate (the error in the limiting value of W is less than 1 % and the error in the critical aspect ratio is less than 2 %). Furthermore, it was shown that Taylor's solution is quite accurate even for the unstable branch unless the deformation is extremely large (accurate at least up to the aspect ratio $a/b = 3$). On the other hand, as we can see in figure 6, the first-order perturbation solution is accurate only up to $W \approx 0.07$.

The good accuracy of the spheroidal steady solution even for cases of large deformation verifies that the dynamical equation (62) is adequate for the global analysis on the drop dynamics. Now let us see the full dynamics for a given W value. We first define

$$x_1 = a, \quad x_2 = \dot{x}_1 = \dot{a}. \tag{69}$$

Then, we have

$$\dot{x}_1 = x_2 \equiv f_1(x_1, x_2), \tag{70a}$$

$$\dot{x}_2 = \frac{4x_1^2}{2x_1^3+1}\left[\tfrac{1}{2}WE^2_{n,\,pole} + \left(\frac{3}{8}\right)\frac{x_2^2}{x_1^3} - \left(\frac{15}{2}\right)S\frac{x_2}{x_1} - 2x_1^2 + \frac{1}{x_1^5} + x_1^{\frac{1}{2}}\right]. \tag{70b}$$

$$\equiv f_2(x_1, x_2).$$

For an inviscid conducting drop ($S = 0$), the phase-plane portraits for the drop dynamics are shown in figure 7 for sub- and supercritical Weber numbers. As we may see, the domain in each phase-plane is decomposed into two parts, stable and unstable regions, by a separatrix when the Weber number is subcritical. Thus, a drop may break up even in the case of a subcritical Weber number if the initial condition is outside the

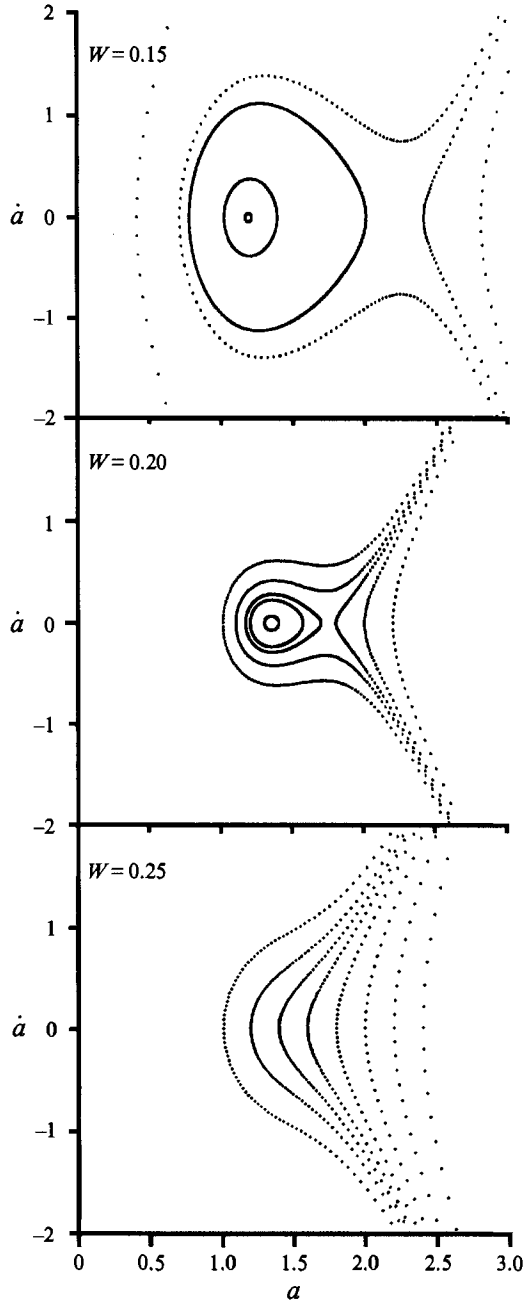

FIGURE 7. Dynamics of a conducting drop in a steady electric field.

separatrix. This is obviously nonlinear dynamical behaviour. In fact, there is an interesting comment on this behaviour: Taylor (1964) explained the experimental data on the drop stability, which is about 7% lower than the predicted critical value of W, as follows: 'The discrepancy may well be due to the fact that Macky's drop suddenly entered the electric field, dropping into it from an unelectrified region, so that they were not in a static stage.'

As will be shown later, the existence of a separatrix has an important meaning for the dynamics of a drop in a time-dependent electric field. Here a comment must be made regarding the term 'breakup'. In fact, the dynamical equation predicts indefinite extension (not real breakup) if the initial condition is outside the separatrix. However, an indefinitely extended drop is expected to be broken up (or disintegrated) at some stage due to the action of surface tension. Hereafter, the term 'breakup' should be understood in that context.

Before going on to the dynamics in a time-periodic electric field, we study the linear stability of the steady-state solution for the system (70). If we define $u_i = x_i - x_{is}, i = 1,2$ and $\boldsymbol{u} = (u_1, u_2)^T$, where x_{is} is the steady-state solution, for the linear stability analysis we have

$$\dot{\boldsymbol{u}} = \boldsymbol{J}\boldsymbol{u}, \tag{71}$$

where $\boldsymbol{J}$ is a Jacobian matrix which is defined by $J_{ij} = \partial f_i/\partial x_j|_{x_s}$. From the eigenvalues of $\boldsymbol{J}$, we may compute the frequency of oscillation and the damping factor as functions of W and S. The results are given in figures 2 and 3 in the earlier §3 for comparison with the results from the perturbation analysis. For the case of inviscid drop ($S = 0$), the same result was obtained earlier by Brazier-Smith *et al.*, who used the linearized version of the dynamical equation.

6. Dynamics of a drop in a time-periodic electric field

For the case of steady electric field at a subcritical Weber number with $S = 0$, the system (70) is a Hamiltonian system with a saddle point and a centre (or elliptic point) (see the phase-plane portrait in figure 7). Now, we are interested in the cases where the Weber number is given as a function of time as

$$W(t) = W_0(1 \pm \tilde{\epsilon}\cos\omega t). \tag{72}$$

A dynamical system with time-periodic forcing can be best studied by a Poincaré map. A Poincaré map is a phase-plane portrait for which the data are taken only at times that are multiples of the period of forcing, i.e. $t = nT, n = 1,2,3,\ldots$. Thus the Poincaré map for an unperturbed Hamiltonian system is identical to the original phase-plane portrait. As is well known from the Kolmogorov–Arnold–Moser (KAM) theorem (see Guckenheimer & Holmes 1983), almost all of the closed curves in the unperturbed Poincaré map are preserved when $\tilde{\epsilon}$ is small. This is especially the case near the elliptic point, so let us start our discussion with the regular orbital dynamics near this point.

6.1. *Regular dynamics near the centre*

In this section, we consider the dynamical behaviour of (70) near the elliptic point when the time-dependent Weber number is given as in (72). We first analyse the dynamics via classical perturbation techniques, and compare the results with numerically constructed Poincaré maps. For a time-periodic Weber number, (70) becomes

$$\dot{x}_1 = x_2, \tag{73a}$$

$$\dot{x}_2 = \frac{4x_1^2}{2x_1^3+1}\left[\tfrac{1}{2}W_0 E_{n,\,pole}^2 + \frac{3}{8}\frac{x_2^2}{x_1^3} - \frac{15}{2}S\frac{x_2}{x_1} - 2x_1^2 + \frac{1}{x_1^{\frac{5}{2}}} + x_1^{\frac{1}{2}}\right]$$

$$\pm\tilde{\epsilon}\left[\frac{2x_1^2}{2x_1^3+1}\right]W_0 E_{n,\,pole}^2\cos\omega t. \tag{73b}$$

Although (73) is a system of ordinary differential equations, it is quite difficult to obtain some analytical results for the dynamical behaviour. Thus, we want to use a simplified version of (73). In order to do that we consider disturbance variables u_1, u_2 defined earlier in (71) and expand (73) up to $O(u_1^2)$, $O(u_1 u_2)$, $O(u_2^2)$ and to $O(\tilde{\epsilon})$. Then

$$\dot{u}_1 = u_2, \tag{74a}$$

$$\dot{u}_2 = -\omega_0^2 u_1 - SDu_2 + Au_1^2 + Bu_2^2 - SCu_1 u_2 \pm \tilde{\epsilon} FW_0 \cos \omega t, \tag{74b}$$

where ω_0 is the frequency of oscillation for an inviscid drop about the steady shape in a steady electric field, i.e. the frequency predicted by (71) when $\tilde{\epsilon} = 0$ and $S = 0$. Thus, $\omega_0 = \omega_0(W_0)$ and it is the frequency obtained by Brazier-Smith *et al.* In (74), the coefficients are defined as

$$A = \frac{1}{2}\frac{\partial^2 f_2}{\partial x_1^2}, \quad B = \frac{1}{2}\frac{\partial^2 f_2}{\partial x_2^2}, \quad C = \frac{\partial}{\partial x_1}\left(\frac{30x_1}{2x_1^3+1}\right),$$

$$D = \frac{30x_1}{2x_1^3+1}, \quad F = \left(\frac{2x_1^2}{2x_1^3+1}\right) E_{n,\,pole}^2.$$

In the above, all coefficients are evaluated at the steady solution (x_{1s}, x_{2s}) for $\tilde{\epsilon} = 0$. For convenience, we define $u = u_1, \dot{u} = u_2$; then (74) may be expressed as

$$\ddot{u} + SD\dot{u} + \omega_0^2 u - Au^2 - B\dot{u}^2 + SCu\dot{u} = \pm \tilde{\epsilon}(FW_0)\cos \omega t. \tag{75}$$

In (75), we consider two perturbation parts, $\pm\cos\omega t$: there is only a phase difference of π between $\cos\omega t$ and $-\cos\omega t$, thus for convenience we confine our discussion to the case of $\cos\omega t$ for the moment.

In Kang & Leal (1990), a similar equation that does not include the $\dot{u}^2$ term has already been discussed in detail for the dynamics of a bubble in straining flows near the critical point. In fact, the term with $\dot{u}^2$ does not have significant effect on the dynamics near the critical point (i.e. $W \sim W_c$), where W_c refers here to the limiting value of W for the existence of steady solution (see figure 6). For that case, $\omega_0^2 \to 0$ as $W \to W_c$ because the frequency of oscillation should be zero at $W = W_c$. (At the critical point $W = W_c$, both eigenvalues of $\boldsymbol{J}$ in (71) are zero when $S = 0$.) But the $\ddot{u}$ term should be balanced by the $\omega_0^2 u$ term, and $\ddot{u} = O(\omega_0^2)\,O(u)$ and $\dot{u} = O(\omega_0)\,O(u)$. Thus, $|\dot{u}^2| \ll |u^2|$ as $W \to W_c$, which means that the term with $\dot{u}^2$ is negligible compared with other terms when $W \to W_c$. However, in the present case, we do not limit our concern to the case of $W \to W_c$. Instead, we consider the dynamics of a drop near the stable state up to the square terms for the whole Weber number region.

6.1.1. *Resonant case* ($\omega \sim \omega_0$)

Now, let us consider the resonant case where the forcing frequency is near the intrinsic frequency of oscillation in a steady electric field, i.e. $\omega \sim \omega_0$. For simplicity, we consider only the inviscid case (i.e. $S = 0$), and we define $\epsilon = \tilde{\epsilon}(FW_0)$. Then (75) becomes

$$\ddot{u} + \omega_0^2 u - Au^2 - B\dot{u}^2 = \epsilon \cos \omega t. \tag{76}$$

Let us first consider the dynamics in the perfect resonance case (i.e. $\omega = \omega_0$). For this end, the two-timing method provides a powerful tool and the leading-order solution is found to be (see references such as Nafeh & Mook 1979)

$$u(t) \sim \epsilon^{\frac{1}{3}} R(\tau)\cos(\omega t - \phi(\tau)), \tag{77}$$

where $\tau = \epsilon^{\frac{2}{3}} t$, and $R(\tau)$, $\phi(\tau)$ satisfy the set of equations

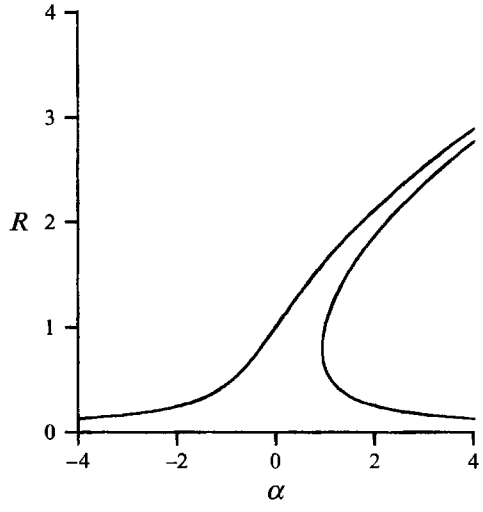

FIGURE 8. Solutions of equation (86) for the case $R_0 = 1$ and $\omega = 1$.

$$\frac{dR}{d\tau} = \frac{1}{2\omega}\sin\phi, \tag{78a}$$

$$R\frac{d\phi}{d\tau} = \frac{(5A^2+5AB\omega^2+2B^2\omega^4)R^3}{12\omega^3} + \frac{\cos\phi}{2\omega}. \tag{78b}$$

One immediate conclusion that can be drawn from (77) is that an $O(\epsilon^{\frac{1}{3}})$ dynamical output is produced by the $O(\epsilon)$ resonant forcing. As will be shown shortly, this behaviour is due to the quadratic terms in (76). In many problems concerning drop or bubble dynamics, the local nonlinear dynamics near the steady solution can be described by the same type of equation as (76). This fact provides a physical significance to the result (77). Whenever we want a large-amplitude oscillation for some reason, we can easily achieve the goal via the resonant forcing.

Although the two-timing solution of (76) can be easily found, in view of the physical significance it is appropriate to show briefly how the $O(\epsilon^{\frac{1}{3}})$ output results from the $O(\epsilon)$ forcing. We expect a bounded two-timing solution of (76) in the form

$$\begin{aligned} u(t) &= \epsilon^p R(\tau)\cos(\omega t - \phi(\tau)) + \epsilon^{2p}u^{(2)}(t,\tau) + \epsilon^{3p}u^{(3)}(t,\tau) + \dots \\ &= \epsilon^p u^{(1)}(t,\tau) + \epsilon^{2p}u^{(2)}(t,\tau) + \epsilon^{3p}u^{(3)}(t,\tau) + \dots, \end{aligned} \tag{79}$$

where $\tau = \epsilon^q t$. Then the quadratic nonlinear terms do not produce the so-called secular terms at $O(\epsilon^{2p})$ but they do at $O(\epsilon^{3p})$. On the other hand,

$$\ddot{u} = \epsilon^p \frac{\partial^2 u^{(1)}}{\partial t^2} + \epsilon^{2p}\frac{\partial^2 u^{(2)}}{\partial t^2} + \epsilon^{p+q}\frac{\partial^2 u^{(1)}}{\partial\tau\partial t} + \dots. \tag{80}$$

Thus $\ddot{u}$ produces a secular term at $O(\epsilon^{p+q})$. In order to have a bounded solution for $u^{(3)}(t,\tau)$, the secular terms produced must be combined with the $O(\epsilon)$ forcing term to eliminate all secular terms. Hence

$$3p = 1, \quad p+q = 1$$

and we have the scalings in (77).

Now let us consider the effect of forcing frequency near the resonant frequency. To do that we introduce the following scaling:†

$$\omega - \omega_0 = -\epsilon^{\frac{2}{3}}\alpha. \tag{81}$$

Then (76) becomes

$$\ddot{u} + (\omega + \epsilon^{\frac{2}{3}}\alpha)^2 u - Au^2 - B\dot{u}^2 = \epsilon \cos \omega t. \tag{82}$$

The equation (82) has a two-timing solution which is again given as (77), but this time $R(\tau)$ and $\phi(\tau)$ should satisfy the following set of equations:

$$\frac{\mathrm{d}R}{\mathrm{d}\tau} = \frac{1}{2\omega} \sin \phi, \tag{83a}$$

$$R\frac{\mathrm{d}\phi}{\mathrm{d}\tau} = \frac{(5A^2 + 5AB\omega^2 + 2B^2\omega^4)\, R^3}{12\omega^3} + \frac{\cos \phi}{2\omega} - \alpha R. \tag{83b}$$

Thus, the effect of forcing frequency change is shown in the leading-order solution through the parameter α in (83*b*).

The fixed point of (83) is determined from the pair of equations

$$\sin \phi = 0, \quad \frac{(5A^2 + 5AB\omega^2 + 2B^2\omega^4)\, R^3}{6\omega^2} - 2\alpha\omega R = -\cos \phi. \tag{84a, b}$$

For convenience, we define R_0 as

$$R_0 \equiv \left\{ \frac{6\omega^2}{5A^2 + 5AB\omega^2 + 2B^2\omega^4} \right\}^{\frac{1}{3}}. \tag{85}$$

Then, since $\cos \phi = \pm 1$ at the fixed point (84*b*) becomes

$$\frac{R^3}{R_0^3} - 2\alpha\omega R = \pm 1, \tag{86}$$

where $+$ is for $\phi = \pi$ and $-$ for $\phi = 0$. The cubic equation (86) has an interesting solution feature depending on the parameter α, as shown in figure 8. The upper and lower curves in figure 8 are for the $+$ and $-$ cases respectively. As we can see from (86) and figure 8, if $\alpha < \alpha_c = (3/2^{\frac{4}{3}})(R_0/\omega)$ only one solution (denoted by R_+^*) on the upper curve exists. However, if $\alpha > \alpha_c$ three solutions exist; one (R_+^*) on the upper curve, and the other two ($R_{-_1}^*$ and $R_{-_2}^*$) on the lower curve. Thus, if $\alpha < \alpha_c$, there is only one fixed point at $(R, \phi) = (R_+^*, \pi)$. On the other hand, if $\alpha > \alpha_c$ there are three fixed points at (R_+^*, π), $(R_{-_1}^*, 0)$, and $(R_{-_2}^*, 0)$. Since R_+^* is a monotonic increasing function of α, we may conclude that the resonance effect becomes stronger as α increases. In other words, the resonance effect is stronger at a slightly lower forcing frequency than at the perfect resonance value (note that α is defined as $\omega - \omega_0 = -\epsilon^{\frac{2}{3}}\alpha$). This point will be verified later by the numerical solution of the full dynamical system (73). Hereafter, we limit our discussion to the upper solution curve because it includes the point $\alpha = 0$ and it corresponds to the strongest resonance. We drop also the subscript $+$ of R_+^* to have the simpler notation R^*. Then the fixed point is at $(R, \phi) = (R^*, \pi)$ for the $\epsilon \cos \omega t$

† This scaling was suggested by one of the referees. The author acknowledges the suggestion.

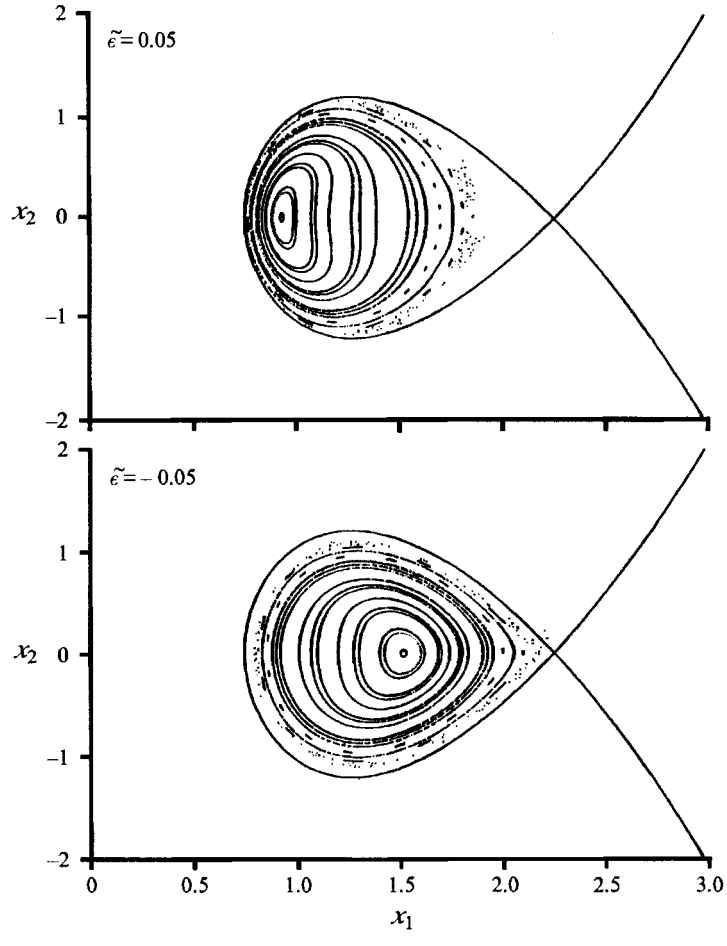

FIGURE 9. Poincaré maps for the exact resonant forcing when $W_0 = 0.15$ ($\omega = \omega_0 = 2.074$, and $\tilde{\epsilon} = \pm 0.05$).

forcing. Since there is only a phase shift of π for the case of $-\epsilon\cos\omega t$ forcing, the fixed point is at $(R^*, 0)$ for the $-\epsilon\cos\omega t$ forcing.

One more point to be mentioned is that the effect of $B\dot{u}^2$ term vanishes as $\omega \to 0$, i.e., as $W \to W_c$ (see (84)). Therefore, as mentioned earlier in Kang & Leal (1990), the qualitative dynamical behaviour of a drop in a time-periodic electric field should be the same as that of a bubble in a time-periodic straining flow at least near the critical points ($W \sim W_c$).

One of the useful features of the two-timing solution is that it provides the Poincaré map directly. For example, the Poincaré map for (77) is simply obtained by substituting $t = nT$ in (77), where T is the period of forcing, i.e., $T = 2\pi/\omega$. In terms of the original variables, x_1 and x_2, the Poincaré map is given by

$$x_1(nT) = u(nT) + x_{1s} \sim \epsilon^{\frac{1}{3}} R(\tau_n)\cos(\phi(\tau_n)) + x_{1s},$$
$$x_2(nT) = \dot{u}(nT) \sim \epsilon^{\frac{1}{3}}\omega R(\tau_n)\sin(\phi(\tau_n)),$$

where $\tau_n = \epsilon^{\frac{2}{3}}(nT)$. Therefore, we can easily see that the fixed points are shifted in the (x_1, x_2)-Poincaré map by $(-\epsilon^{\frac{1}{3}}R^*, 0)$ for $\epsilon\cos\omega t$ forcing and $(\epsilon^{\frac{1}{3}}R^*, 0)$ for $-\epsilon\cos\omega t$

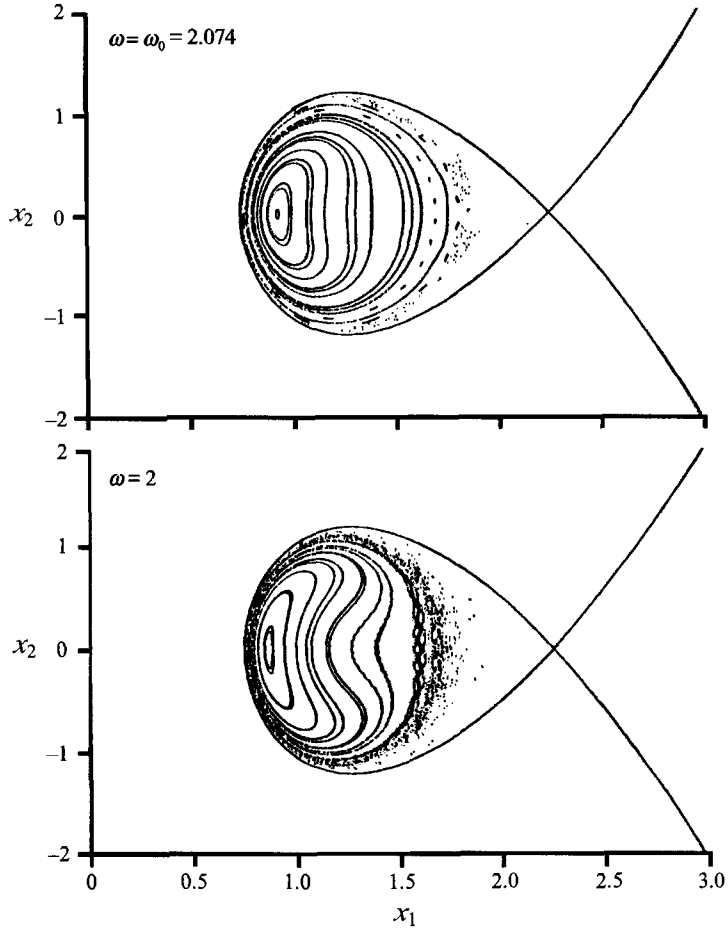

FIGURE 10. Poincaré maps for the cases of exact resonant forcing ($\omega = 2.074$) and nearly resonant forcing ($\omega = 2$) when $W_0 = 0.15$ and $\tilde{\epsilon} = 0.05$.

forcing. Owing to the KAM theorem, there exist closed curves near the fixed point. Figure 9 shows two Poincaré maps generated by numerical integration of the full dynamical system (73) for the resonant case $\omega = \omega_0 = 2.074$ when $W_0 = 0.15$ and $\tilde{\epsilon} = \pm 0.05$ ($\epsilon = \pm 0.05 F W_0$). As predicted above by the two-timing analysis, the fixed points are shifted to the left and to the right by $\epsilon^{\frac{1}{3}} R^*$. One more point to be mentioned on the Poincaré maps is that the Poincaré map for $-0.05\cos\omega t$ corresponds to the Poincaré map for $0.05\cos\omega t$ for which data are taken at $t = (n+\frac{1}{2})T$.

From the two-timing analysis, we have seen that the resonance effect increases as the forcing frequency decreases in the vicinity of the intrinsic frequency. Indeed, this behaviour has been verified by the numerically generated Poincaré map for the full dynamical equation. In figure 10, the Poincaré map for a nearly resonant forcing (slightly lower forcing frequency ($\omega = 2$) than the intrinsic frequency of drop oscillation ($\omega_0 = 2.074$)) is compared with the Poincaré map for resonant forcing when $W_0 = 0.15$ and $\tilde{\epsilon} = 0.05$. As we can see, the resonance effect is stronger at a frequency that is slightly lower than the intrinsic frequency ω_0.

6.1.2. $n = 2$ *resonant case* ($\omega \sim 2\omega_0$)

If the forcing frequency (ω) is far from ω_0, no particularly interesting results are expected near the centre, at least up to the leading-order solution. In fact, the leading-order solution is simply

$$u \sim \epsilon R \cos(\omega_0 t - \phi) + \frac{\epsilon}{\omega_0^2 - \omega^2} \cos \omega t, \tag{87}$$

where R and ϕ are constants that must be determined from the initial conditions. However, if we consider the next-order term, it is clear that there is again a multiple timescale response for the cases $\omega \sim 2\omega_0$ and $\omega \sim \frac{1}{2}\omega_0$. In particular, for these cases the nonlinear terms in (75) produce secular terms that must be suppressed in order to have bounded solutions at the second-order approximation. Since the $\omega \sim 2\omega_0$ case exhibits interesting behaviour, we briefly consider it below.

For convenience in analysis, we define $\tilde{\omega} = \frac{1}{2}\omega$ and assume $\omega_0 = \tilde{\omega} + \epsilon\alpha$, where α is an $O(1)$ constant. Then (76) becomes

$$\ddot{u} + (\tilde{\omega} + \epsilon\alpha)^2 u - Au^2 - B\dot{u}^2 = \epsilon \cos 2\tilde{\omega} t. \tag{88}$$

In this case, (87) is modified for the case $\omega \sim 2\omega_0$ to the form

$$u \sim \epsilon R(\tau) \cos(\tilde{\omega} t - \phi(\tau)) - \frac{\epsilon}{3\tilde{\omega}^2} \cos 2\tilde{\omega} t, \tag{89}$$

where $\tau = \epsilon t$. It can be shown that the functions $R(\tau)$ and $\phi(\tau)$ satisfy the dynamical equations

$$\frac{\mathrm{d}R}{\mathrm{d}\tau} = -\left(\frac{A}{6\tilde{\omega}^3} + \frac{B}{3\tilde{\omega}}\right) R \sin 2\phi \equiv -\beta R \sin 2\phi, \tag{90a}$$

$$\frac{\mathrm{d}\phi}{\mathrm{d}\tau} = \left(\frac{A}{6\tilde{\omega}^3} + \frac{B}{3\tilde{\omega}}\right) \cos 2\phi + \alpha \equiv \beta \cos 2\phi + \alpha. \tag{90b}$$

As expected, (90) has a fixed point at $R = 0$, which can be either a saddle point or a centre in the $(R\cos\phi, R\sin\phi)$-plane depending on the value of $|\alpha/\beta|$. If $|\alpha/\beta| > 1$, then ϕ is a monotonic function of τ, and (90) has an integral

$$R^2 = c|\beta \cos 2\phi + \alpha|,$$

where c is a positive number that depends on the initial condition. Therefore $R = 0$ is a centre. On the other hand, if $|\alpha/\beta| < 1$, then $\mathrm{d}\phi/\mathrm{d}\tau = \beta \cos 2\phi + \alpha = 0$ has four solutions in $0 \leqslant \phi \leqslant 2\pi$. Along these lines $\mathrm{d}R/\mathrm{d}\tau < 0$ or $\mathrm{d}R/\mathrm{d}\tau > 0$, thus $R = 0$ is a saddle point.

As in §6.1.1, the Poincaré map for (88) near the centre can be predicted by (89) by substituting $t = nT$ where $T = 2\pi/\omega = \pi/\tilde{\omega}$. Thus, the fixed point in the Poincaré map is either a centre or a saddle point depending on the parameter values. Indeed, the natures of the fixed point predicted by the two-timing analysis can be verified by the Poincaré maps for the full dynamical equation. In figure 11, there are two Poincaré maps generated by numerical integration of (73) for $W_0 = 0.15$ with the forcing frequencies of $\omega = 2\omega_0 = 4.148\,(\alpha = 0)$ and $\omega = 2(\omega_0 - 0.074) = 4\,(|\alpha/\beta| > 1)$. As expected, the fixed point for the $\alpha = 0$ case is a saddle point while the fixed point for the $|\alpha/\beta| > 1$ case is a centre point in the $(R\cos\phi, R\sin\phi)$-plane.

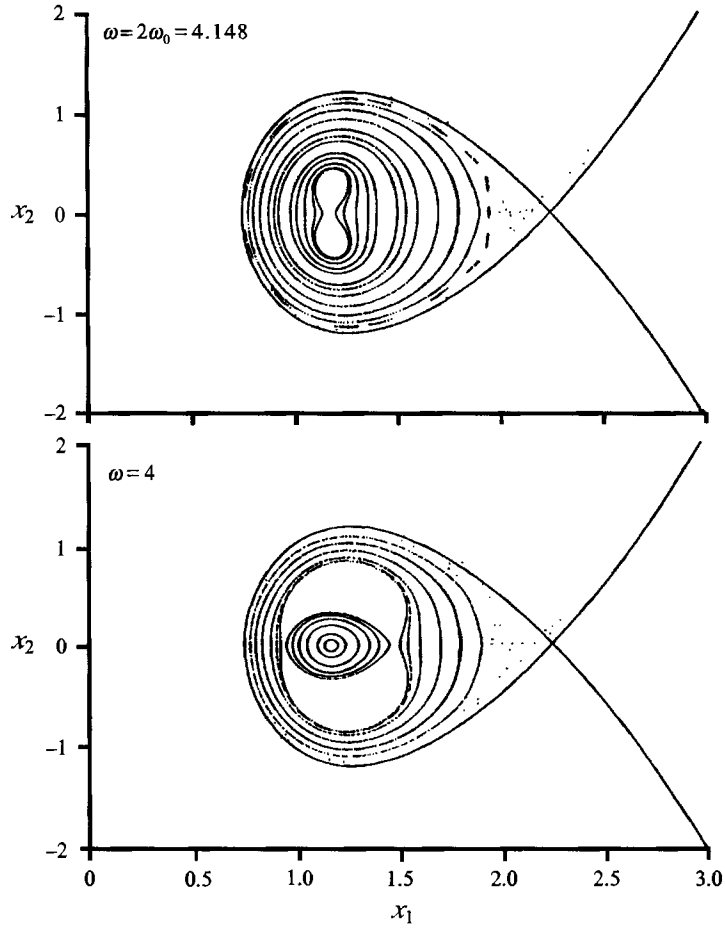

FIGURE 11. Poincaré maps for the exact $n = 2$ resonant forcing ($\omega = 2\omega_0 = 4.148$) and the nearly $n = 2$ resonant forcing ($\omega = 4$) when $W_0 = 0.15$ and $\tilde{\epsilon} = 0.1$.

6.2. *Chaotic drop dynamics and breakup*

Chaotic dynamics resulting from homoclinic orbit tangling for a perturbed two-dimensional map is well explained elsewhere (cf. Guckenheimer & Holmes 1983 or Wiggins 1988). As mentioned earlier, the drop dynamics in an electric field is very similar to the bubble dynamics in a straining flow, and the effect of time-periodic forcing on drop breakup may be similarly understood by the lobe dynamics in Kang & Leal (1990) (see also recent papers by Rom-Kedar & Wiggins 1990 and McRobie & Thompson 1991). So here we touch only on the condition for the chaotic dynamics to occur and the specific Poincaré maps for the drop dynamics in a time-periodic electric field.

For the case of $S = 0$, the Poincaré map of (73) always has a homoclinic tangle, but if $S > 0$ a homoclinic tangle (i.e. chaotic drop dynamics) is not always possible. In order to have a homoclinic tangle, the ratio of the amplitude of forcing to the damping coefficient S must exceed a certain critical value, which is a function of the forcing frequency. The condition for chaotic drop dynamics (or equivalently the existence of a homoclinic tangle) for $\tilde{\epsilon} \ll 1$ can be obtained via the Melnikov function (cf. Guckenheimer & Holmes). The Melnikov function essentially provides a measure of

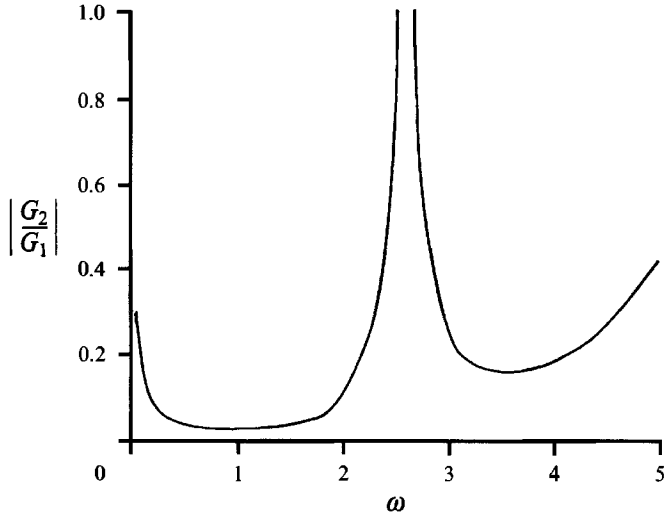

FIGURE 12. The condition for existence of homoclinic tangle for $S > 0$; $W = 0.15$.

the separation between the stable and unstable manifolds in the phase plane. Hence, when the Melnikov function equals zero, the stable and unstable manifolds intersect. For the system (73), the Melnikov function can be computed by

$$M(t_0) = \int_{-\infty}^{\infty} x_2 \left[W \cos\omega(t+t_0) \frac{E^2_{n,pole}(2x_1^2)}{2x_1^3+1} - \frac{15S}{\tilde{\epsilon}} \frac{2x_1 x_2^2}{2x_1^3+1} \right] \mathrm{d}t$$

$$= 2W_0 \sin\omega t_0 \int_0^{\infty} \frac{E^2_{n,pole}(2x_1^2 x_2)\sin\omega t}{2x_1^3+1} \mathrm{d}t - \frac{30S}{\tilde{\epsilon}} \int_0^{\infty} \frac{2x_1 x_2^2}{2x_1^3+1} \mathrm{d}t$$

$$\equiv 2W_0 \sin\omega t_0 \, G_1 - \frac{30S}{\tilde{\epsilon}} G_2, \tag{91}$$

where G_1 and G_2 are functions of ω and evaluated numerically. The condition for existence of a homoclinic tangle, obtained from the Melnikov function equal to zero, is

$$\frac{1}{15}\left(\frac{\tilde{\epsilon} W_0}{S}\right) > \left|\frac{G_2}{G_1}\right|. \tag{92}$$

In figure 12, $|G_2/G_1|$ is plotted for $W_0 = 0.15$. For $W_0 = 0.15$, the intrinsic frequency of oscillation is $\omega_0 = 2.074$. Thus, $|G_2/G_1|$ has a minimum value at the frequency of $\omega \sim 0.5\,\omega_0$, which means that for a given S value, chaotic drop dynamics may occur at the smallest value of $|G_2/G_1|$.

As mentioned earlier, the dynamics of a drop in a time-periodic electric field may be best understood by the Poincaré maps. For that end, Poincaré maps are generated by numerical integration of the dynamical system (73) for various frequencies and amplitudes of time-periodic forcing.

We have first studied the effect of forcing amplitude on the drop dynamics for a fixed, nearly resonant frequency ($\omega = 2$ when $W_0 = 0.15$ and $\omega_0 = 2.074$). As mentioned earlier in §6.1.2, the resonant effect is stronger when the forcing frequency is slightly lower than the resonant frequency predicted by the linear analysis. Thus, we have chosen the forcing frequency as $\omega = 2$ rather than the exact resonant frequency

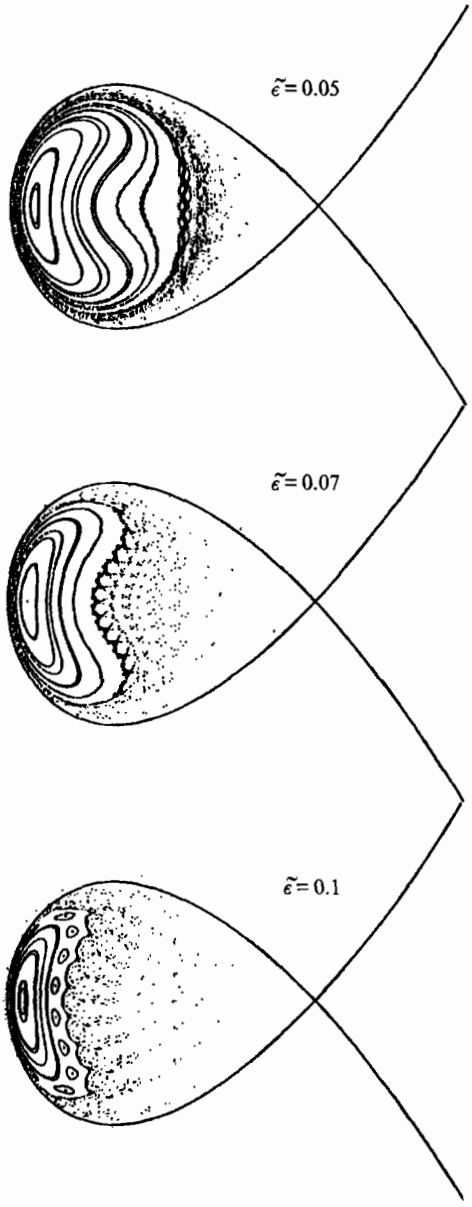

FIGURE 13. The effect of forcing amplitude on the Poincaré maps in the nearly resonant case ($\omega = 2 \sim \omega_0$ and $W_0 = 0.15$).

$\omega = \omega_0 = 2.074$. The effect of forcing amplitude for the resonant case ($\omega = 2 \sim \omega_0$) is shown in figure 13. As expected, the regular region shrinks in size as the forcing amplitude increases. (In each Poincaré map, the separatrix for the case of steady electric field ($W = W_0 = 0.15$) is also shown for reference.)

A conducting drop exhibits quite different behaviour depending on whether it is initially in the regular region or chaotic region. In figure 14, the effect of initial conditions on the drop dynamics for the resonant case ($\omega = 2, \tilde{\epsilon} = 0.05$) is shown. As expected, a drop shows a two-timing behaviour when the initial condition is in the regular region ($x_{10} = 1.01$ and $x_{20} = 0$). On the other hand, when we changed x_{10} to 1.8,

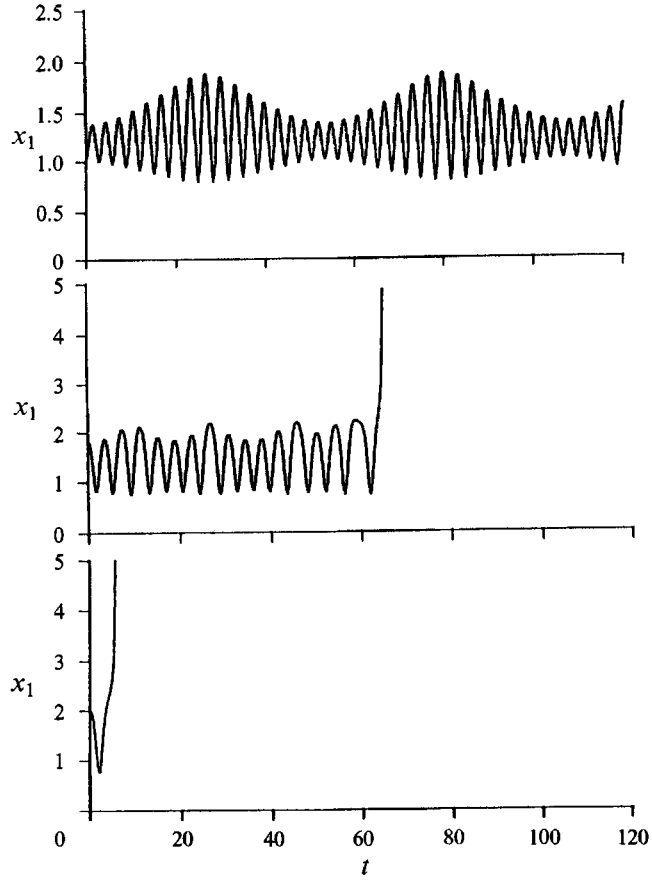

FIGURE 14. The effect of initial conditions on the drop dynamics for the case of nearly resonant forcing ($\omega = 2$, $\tilde{\epsilon} = 0.05$, and $W_0 = 0.15$).

the drop oscillates chaotically for a while and finally breaks up. This chaotic breakup can be best understood by the lobe dynamics such as in Kang & Leal (1990) or McRobie & Thompson (1991). When we further increase x_{10} to 2.0, we observe an earlier breakup as we can see in figure 14. As we have noticed above, a drop does not break up if it is initially in the regular region, otherwise it eventually breaks up. Thus, the size of the regular region can serve as a measure of drop breakup efficiency. From figure 13, we can observe that the breakup efficiency is significantly improved by resonant forcing. Particularly, it is noteworthy that considerable shrinkage of the regular region can be obtained by resonant forcing with small amplitude.

As mentioned earlier, one of the most critical factors in drop dynamics is the forcing frequency. In figure 15, the effect of the forcing frequency on the Poincaré maps is shown for the case of $W_0 = 0.15$, $\tilde{\epsilon} = 0.1$. As expected, the regular region has the minimum size when the forcing frequency is near the resonant value. The effect of the forcing frequency can also be shown by the plots of x_1 *vs.* t shown in figure 16. For the same $W_0 = 0.15$, $\tilde{\epsilon} = 0.05$, and $x_{10} = 1.2$, $x_{20} = 0$, the forcing frequency was varied. As we can see, the $O(\tilde{\epsilon}^{\frac{1}{3}})$ output was produced by the $O(\tilde{\epsilon})$ forcing when the forcing is near the resonant value, while only $O(\tilde{\epsilon})$ output was obtained for the non-resonant cases.

Thus far, we have discussed the dynamics of an inviscid drop in a time-periodic electric field. Here, we want to show that a viscous drop can also be effectively broken

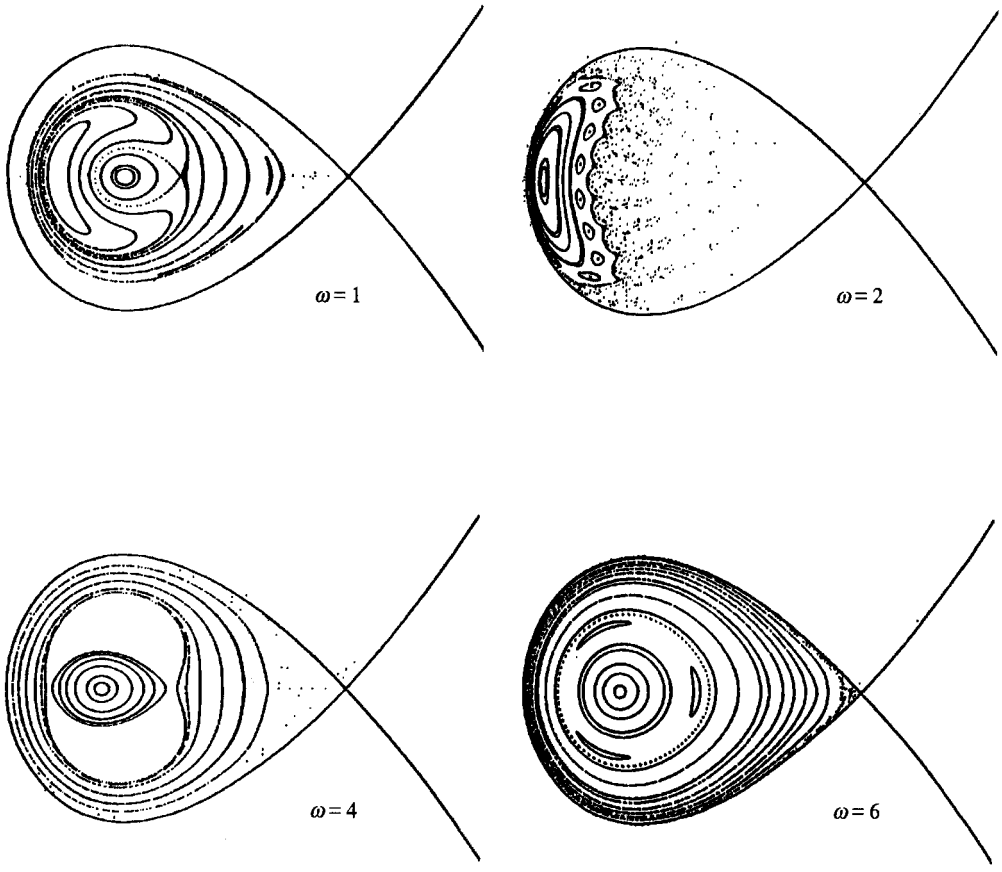

FIGURE 15. The effect of forcing frequency on the Poincaré maps when $W_0 = 0.15$ and $\tilde{\epsilon} = 0.1$.

up by resonant forcing. In our analysis, the viscous effect is represented by the dimensionless number S defined in §2. Before starting our discussion, let us first look at some typical values of S. If we assume $\mu = 0.01$ g cm^{-1} s^{-1}, $\rho = 1$ g cm^{-3}, and $\gamma = 70$ dyne cm^{-1} for an aqueous drop, then $S = 1.2 \times 10^{-3}$ for $a_0 = 1$ cm, $S = 1.2 \times 10^{-2}$ for $a_0 = 10^{-2}$ cm, and $S = 1.2 \times 10^{-1}$ for $a_0 = 10^{-4}$ cm. Note that the value of S is small enough even for extremely small droplets of size 1 μm. Thus, we may safely assume that the weak viscous effect is valid for most cases. In order to see the resonant breakup phenomena of a weakly viscous drop, which is initially at rest ($x_{10} = 1.01$), alternating electric fields are considered. In this case, the time-dependent Weber number may be described as $W(t) = W_0(1 + \cos \omega_{res} t)$, where ω_{res} is the intrinsic resonance frequency of a drop in a steady electric field of $W = W_0$. As we have seen in §3.1, the intrinsic frequency predicted by the theory based on the spheroidal approximation agrees very well with the prediction by the asymptotic formula (37) when $W \leqslant 0.12$ and $S = 0$. Thus, this time the asymptotic formula (37) with $S = 0$ (which is the same as Feng's asymptotic formula) was used with $n = 2$ to produce $\omega_{res}^2 = 8 - 22.114 W_0$. Resonant drop breakup phenomena are shown in figure 17 for $S = 0$, 0.01, and 0.1. For each S value, W_0 was adjusted to the nearly minimal value for which resonant breakup is possible. From figure 17, we can see the fact that the breakup efficiency can be significantly improved by applying a resonant electric field. When a steady electric field is applied, drop breakup is possible at the value of

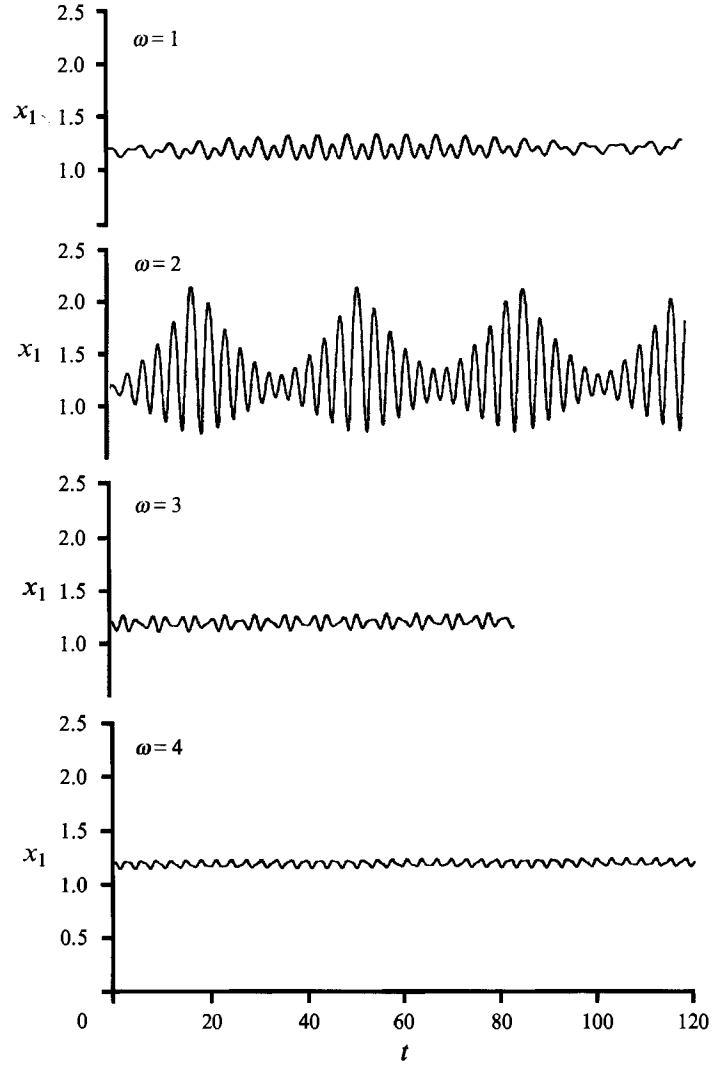

FIGURE 16. The effect of forcing frequency on the drop dynamics when $W_0 = 0.15$.

$W \geqslant 0.188$ for $S = 0$, $W \geqslant 0.189$ for $S = 0.01$, and $W \geqslant 0.21$ for $S = 0.1$. (For a steady electric field, a drop always breaks up if $W \geqslant 0.21$. But, when S is very small, breakup can also be possible at smaller values due to the nonlinear effect. In particular, when $S = 0$, a drop breaks up in a steady field if its initial condition is outside the separatrix. For $0.188 \leqslant W < W_c$, the size of separatrix is small enough for $(x_{10}, x_{20}) = (1.01, 0)$ to be outside the separatrix. See the phase-plane portraits in figure 7.) On the other hand, when the resonant alternating field is applied, breakup is possible at the average value of $W_0 \geqslant 0.01$ for $S = 0$, $W_0 \geqslant 0.04$ for $S = 0.01$, and $W_0 \geqslant 0.14$ for $S = 0.1$.

6.3. *Discussion of the results*

In the present work, drop dynamics in a time-dependent electric field has been investigated via analyses of the dynamical equation derived with the spheroidal approximation. As mentioned earlier, the dynamical equation cannot represent the exact dynamical behaviour of a conducting drop in various time-dependent electric

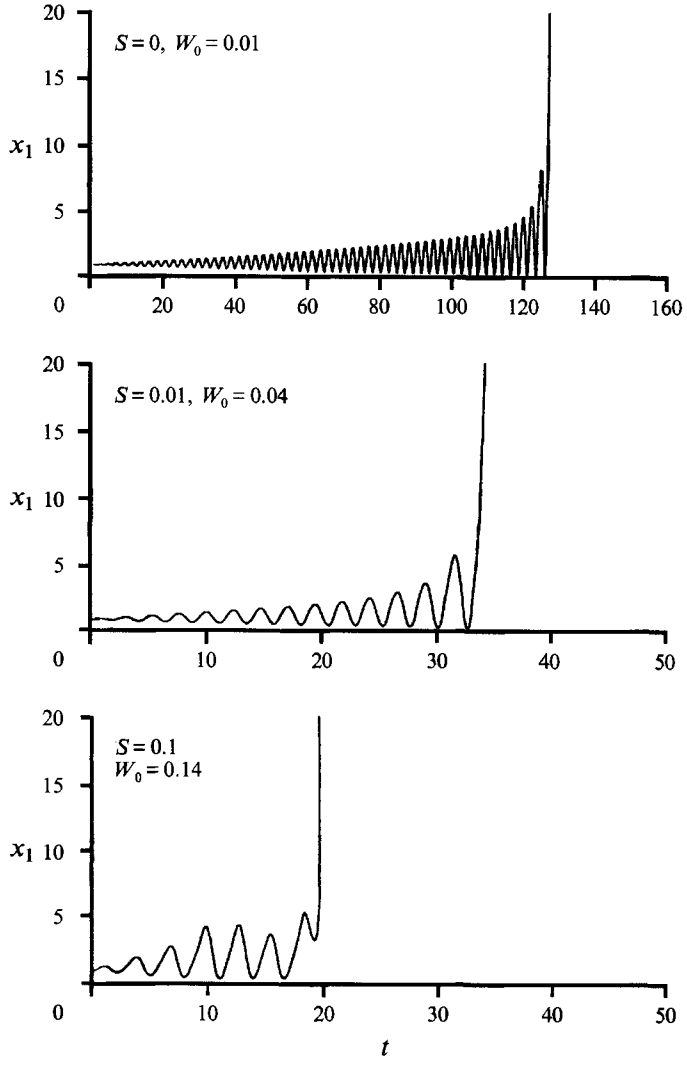

FIGURE 17. Drop breakup by resonant alternating electric fields for the cases $S = 0$, 0.01 and 0.1.

fields. However, as far as stretching and breakup of a drop are concerned, the dynamical equation is believed to represent the real dynamics quite well if we interpret exponential stretching as drop breakup. In the dynamical equation, we assume that a drop takes a prolate spheroidal shape even if the drop is extended indefinitely. However, in a real situation the drop will surely break up due to the action of surface tension.

Since the validity of the dynamical equation depends significantly on the accuracy of its steady-state solutions, let us take a look at the steady-state solutions. As commented in Taylor (1964), the steady-state solution on the stable branch is very accurate. For unstable steady-state solutions, Miksis (1981) and Basaran & Scriven (1989) showed that the unstable equilibrium shapes predicted by the spheroidal approximation agree quite well with the numerical results if $|W - W_c|$ is not so large. We have also checked the relative normal stress imbalance $([\hat{\boldsymbol{n}}\cdot\hat{\boldsymbol{n}}\cdot\boldsymbol{T}] - \nabla\cdot\hat{\boldsymbol{n}})/\nabla\cdot\hat{\boldsymbol{n}}$ at each point on the spheroidal surface. In figure 18, the relative normal stress imbalance is

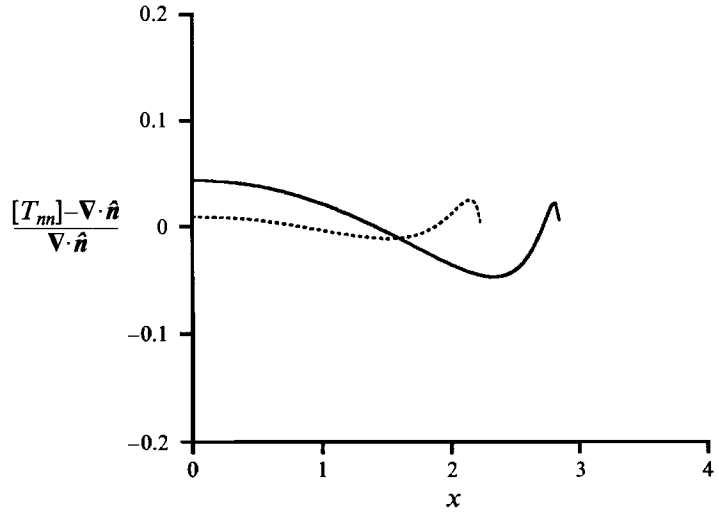

FIGURE 18. Relative normal stress imbalance $([\hat{n}\cdot\hat{n}\cdot T]-\nabla\cdot\hat{n})/\nabla\cdot\hat{n}$ at the drop surface of the unstable steady-state solutions (dotted line: $W = 0.15$; solid line: $W = 0.1$).

shown for the unstable steady-state solutions at $W = 0.15$ (dotted line) and $W = 0.1$ (solid line). As we can see, the normal stress condition is satisfied within few percent error. Thus, we may say that the exact solution is not far from the spheroidal shape if $W \geqslant 0.1$. Therefore we may assume that the dynamical equation can produce meaningful information on the drop dynamics in both qualitative and quantitative senses if $W \geqslant 0.1$. Of course, the true unstable steady shape may be quite different from a spheroidal shape for very small Weber numbers. For those cases, the results in this paper must be understood only from the qualitative point of view.

7. Concluding remarks

In the present work, the nonlinear dynamical behaviour of a conducting drop in a time-periodic field has been studied. The most important result is the dynamical equation for drop deformation (equation (62)), which was derived in the form of a nonlinear ordinary differential equation based on the spheroidal approximation for the drop shape and the weak viscous effect. Although not exact and not capable of describing modes other than spheroidal deformation, the dynamical equation is believed to represent all possible dynamics of a drop in an arbitrary time-dependent electric field as long as the deformation is in the direction of the imposed field.

Although capable of dealing with any kind of time-dependency of the electric field, the dynamical equation has been analysed for the special cases of time-periodic forcing by using two methods of analysis: classical two-timing analysis and Poincaré map analysis. The two-timing analysis on the dynamical equation revealed that in the neighbourhood of stable-state solution, an $O(\epsilon^{\frac{1}{3}})$ time-dependent change of shape can be obtained from an $O(\epsilon)$ resonant forcing. The analysis also showed that the resonance effect is stronger at a forcing frequency that is slightly lower than the intrinsic frequency of exact resonance. The Poincaré map analysis showed that the probability of drop breakup via chaotic oscillation can be maximized by choosing an optimal frequency for a fixed amplitude in time-periodic forcing. The optimal frequency was found to be the value that is slightly lower than the resonant frequency as predicted by the two-timing analysis.

The $O(\epsilon^{\frac{1}{3}})$ amplification by resonance and breakup via chaotic oscillation seem to represent two of the common characteristics in the problems of drop and bubble dynamics. This is especially the case when the steady-state solutions show the same critical phenomena as in this problem. Such examples include bubble dynamics in a straining flow (Kang & Leal 1990) and bubble oscillation in a time-periodic pressure field (Leal 1992). These common characteristics may be exploited in various applications.

In view of the importance of the correct estimation of the intrinsic frequency of oscillation in a steady field, a brief perturbation analysis has also been performed to extend Feng's (1990) asymptotic formula for the frequency modification by including the weak viscosity effect. Differently from other methods based on the theory of viscous dissipation, the viscous pressure correction and the viscous normal stress have been obtained directly by considering the perturbed velocity field due to weak viscosity. The analysis revealed the physics underlying the damping effect by showing that the viscous pressure correction and the viscous normal stress exert forces on the drop surface in the direction opposite to that of fluid motion.

The author wishes to thank the referees for their valuable suggestions and comments. This work was supported by a grant from the Advanced Fluids Engineering Research Center at the Pohang Institute of Science and Technology.

REFERENCES

BASARAN, O. A. & SCRIVEN, L. E. 1989 Axisymmetric shapes and stability of charged drops in an external electric field. *Phys. Fluids* A **1**, 799–908.

BATCHELOR, G. K. 1967 *An Introduction to Fluid Dynamics*. Cambridge University Press.

BRAZIER-SMITH, P. R., BROOK, M., LATHAM, J., SAUNDERS, C. P. R. & SMITH, M. H. 1971 The vibration of electrified water drops. *Proc. R. Soc. Lond.* A **322**, 523–534.

FENG, J. Q. 1990 A method of multiple-parameter perturbations with an application to drop oscillations in an electric field. *Q. Appl. Maths* **48**, 555–567.

FENG, J. Q. & BEARD, K. V. 1990 Small-amplitude oscillations of electrostatically levitated drops. *Proc. R. Soc. Lond.* A **430**, 133–150.

FENG, J. Q. & BEARD, K. V. 1991*a* Resonances of a conducting drop in an alternating electric field. *J. Fluid Mech.* **222**, 417–435.

FENG, J. Q. & BEARD, K. V. 1991*b* Three-dimensional oscillation characteristics of electrostatistically deformed drops. *J. Fluid Mech.* **227**, 429–447.

GUCKENHEIMER, J. & HOLMES, P. J. 1983 *Nonlinear Oscillations, Dynamical Systems, and Bifurcations of Vector Fields*. Springer.

KANG, I. S. & LEAL, L. G. 1988 Small-amplitude perturbations of shape for a nearly spherical bubble in an inviscid straining flow (steady shapes and oscillatory motion). *J. Fluid Mech.* **187**, 231–266.

KANG, I. S. & LEAL, L. G. 1990 Bubble dynamics in time-periodic straining flows. *J. Fluid Mech.* **218**, 41–69.

LAMB, H. 1932 *Hydrodynamics*, 6th edn. Dover.

LANDAU, L. D. & LIFSHITZ, E. M. 1975 *Electrodynamics of Continuous Media*. Pergamon.

LEAL, L. G. 1992 *Laminar Flow and Convective Processes: Scaling Principles and Asymptotic Analysis*. Butterworth-Heinemann.

MCROBIE, F. A. & THOMPSON, J. M. T. 1991 Lobe dynamics and the escape from a potential well. *Proc. R. Soc. Lond.* A **435**, 659–672.

MELCHER, J. R. & TAYLOR, G. I. 1969 Electrohydrodynamics: a review of the role of interfacial shear stresses. *Ann. Rev. Fluid Mech.* **1**, 111–146.

MIKSIS, M. J. 1981 Shape of a drop in an electric field. *Phys. Fluids* **24**, 1967–1972.

MORRISON, C. A., LEAVITT, R. P. & WORTMAN, D. E. 1981 The extended Rayleigh theory of the oscillation of liquid droplets. *J. Fluid Mech.* **104**, 295–309.

NAFEH, A. H. & MOOK, D. T. 1979 *Nonlinear Oscillations*. Wiley-Interscience.

NAFEH, M. H. & BRUSSEL, M. K. 1985 *Electricity and Magnetism*. John Wiley & Sons.

PROSPERETTI, A. 1977 Viscous effects on perturbed spherical flows. *Q. Appl. Maths* **34**, 339–351.

ROM-KEDAR, V. & WIGGINS, S. 1990 Transport in two-dimensional maps. *Arch. Rat. Mech. Anal.* **109**, 239–298.

SAMPLE, S. B., RAGHUPATHY, B. & HENDRICKS, C. D. 1970 Quiescent distortion and resonant oscillations of a liquid drop in an electric field. *Intl J. Engng Sci.* **8**, 97–109.

SOZOU, C. 1972 Electrohydrodynamics of a liquid drop: the time-dependent problem. *Proc. R. Soc. Lond.* A **331**, 263–272.

TAYLOR, G. I. 1964 Disintegration of water drops in an electric field. *Proc. R. Soc. Lond.* A **280**, 383–397.

TAYLOR, G. I. 1966 The circulation produced in a drop by an electric field. *Proc. R. Soc. Lond.* A **291**, 159–166.

WIGGINS, S. 1988 *Global Bifurcations and Chaos: Analytical Methods*. Springer.